Chapter II

Colorimetric Sensing of Milk Adulterants

CHAPTER II

COLORIMETRIC SENSING OF MILK ADULTERANTS

- *This chapter is subdivided into two parts.*
- *The first part reports colorimetric detection technique for qualitative assessment of melamine, hydrogen peroxide, formalin, and salicylic acid content in raw milk without use of any substrate.*
- *The second part highlights the fabrication of a novel paper-based sensing platform designed for simultaneous colorimetric sensing of various adulterants and contaminants in milk.*
- *Green tea, cotton leaves, l-cysteine, and watermelon rind extract-functionalized silver nanoparticles (AgNPs) were utilised for colorimetric detection of melamine, hydrogen peroxide, formalin, and salicylic acid in milk, respectively.*
- *The limit of detection (LOD) for each sensing architecture was estimated utilising the UV-Visible (UV-Vis) spectra and was found to be 1.44 ppm for melamine, 8.46 ppm for hydrogen peroxide, 3.51 ppm for formalin, and 0.55 ppm for salicylic acid, respectively.*
- *The developed paper-based sensing platform utilizes seven conduits, where each end is selectively impregnated with functionalized AgNPs being separated by hydrophobic barriers.*
- *The system is designed to sense milk adulterants such as melamine, formalin, and hydrogen peroxide and milk contaminants such as mercury, arsenic, cadmium, and lead ions.*
- *Each detection scheme demonstrates remarkably low LOD and high sensitivity.*

2.1 Introduction

Milk adulteration and contamination have been a long-standing challenge faced by society from generations [1]. Adulteration involves the introduction of unwanted foreign substances into milk, compromising its quality and rendering it unsuitable for consumption [2]. On the contrary, milk contamination refers to presence of undesirable foreign elements

in milk which may appear in milk during the pasteurization process, grazing of cattle in mining/ industrial areas, etc [3].

Milk is often adulterated with various types of adulterants, with some used to falsify the net protein content. This includes the addition of toxic nitrogen-rich compounds like melamine and urea [4]. Meanwhile other adulterants such as hydrogen peroxide, formalin, and salicylic acid are mixed to extend shelf life and prevent degradation of milk. All these adulterants are found to be highly toxic and possess carcinogenic effects [5,6].

Diluting milk reduces its protein concentration. The Dumas and Kjeldahl methods are used to determine the total content of protein in milk by estimating the total amount of nitrogen in milk. Melamine contains around (66%) of nitrogen by mass and is therefore used to falsely elevate protein levels by increasing the non-protein nitrogen content in milk. Its consumption on regular basis can lead to development of stones in kidney and may also result in renal failure [4]. Likewise, formalin, hydrogen peroxide and salicylic acid being used as preservatives, are highly toxic and possess carcinogenic effects, which can even cause organ damage over prolonged consumption [5,6].

The addition of these adulterants poses significant health risks and challenges for detection due to their textures and chemical properties [7]. There is an urgent need to develop point-of-care systems which can sense the presence of these adulterants without sophisticated setups thereby facilitating regular monitoring of milk quality.

Meanwhile, milk contamination by heavy metal (HM) residues is another significant issue, where metals ions such as mercury, arsenic, cadmium, and lead are often introduced during the pasteurization process [8,9]. The consumption of these HM ions is dangerous and thus, the regulatory bodies have prescribed their maximum permissible limits. These metals ions are non-biodegradable and over time can accumulate in the human body. This may lead to serious health risks, including neurological disorders, organ failure, kidney damage, and even cause developmental problems in infants and children. The detection of HM contamination in milk are therefore crucial to ensure consumer safety [10].

Of late metal NPs have emerged as a captivating tool for varied colorimetric-based sensing assays due to a unique phenomenon known as localised surface plasmon resonance (LSPR) [11]. AgNPs and gold nanoparticles (AuNPs) are primarily harnessed for designing colorimetric assays owing to their exceptional plasmonic properties in the visible spectrum [12]. AgNPs, in particular, are favoured for their exceptional excitation coefficients and cost-effectiveness [13]. However, their highly unstable nature is a drawback due to their high oxidizing properties. This bottleneck can be mitigated by using suitable functionalizing or capping agents to enhance their stability [14].

Existing literature includes numerous chromatographic techniques for detecting adulterants in milk, but these methods are highly sophisticated and necessitate intricate pretreatment procedures [2,15]. Some colorimetric approaches are also reported but they often entail long pretreatment processes and extended sensing procedures, demanding a substantial amount of chemicals for effective detection [16-20].

Use of plasmonic NPs as colorimetric sensors have gathered the attention of researchers due to their low cost, simplicity, and high specificity [16]. These sensors allow qualitative analysis of the presence of any analyte by observing the colour change in the NP solution with the naked eye. This eliminates the need for sophisticated or expensive devices [18].

Colorimetric sensing can be broadly classified into two domains: aggregation-based and non-aggregation-based colorimetric sensing. In aggregation-based sensing, NPs are surface-functionalized with molecules that enable specific chemical interactions or binding with a particular functional group of the targeted analyte. When the analyte is present, it interacts with the surface-functionalized NPs, causing the interparticle distance between them to decrease. This results in NP aggregation. Aggregation induces a significant shift of the LSPR band of NPs, resulting in a visible colour change in the colloidal NP solution [21]. This is due to the coupling of plasmonic fields between the closely spaced NPs [22]. The aggregation-based colorimetric method can be further classified into two types one of which is rapid aggregation-based colorimetric sensing. In this approach, surface-functionalized NPs quickly interact with the analyte, which promotes aggregation and leads to an immediate colour change. This method is rapid, and

allows real-time detection of analytes, in a variety of sample matrices. Another type of aggregation-based sensing is interference-based aggregation sensing [23]. In this type, the targeted analyte interferes with the synthesis or stability of the NPs, leading to aggregation during the synthesis process itself. For example, some analytes can alter the reduction process during NP formation, resulting in the production of larger or aggregated particles. This process induces a distinct colour change, which can be visually detected. This method is particularly useful for detecting analytes that can influence the chemical conditions under which NPs forms [23].

Another broad classification of colorimetric sensing is non-aggregation-based colorimetric sensing. Here, the analyte induces a chemical transformation of the NPs rather than aggregation [24]. This often involves redox reactions where the analyte, acting as an oxidizing agent, interacts with the NPs and converts back to their ionic forms. This oxidation results in the dissolution of the NPs and a significant shift in colour. This approach is particularly useful when detecting analytes like hydrogen peroxide or other oxidative species [24,25].

Both aggregation-based and non-aggregation-based colorimetric sensors offer distinct advantages depending on the type of analyte and the nature of the detection mechanism, making them versatile tool for various sensing applications.

Some studies reported in the literature have also demonstrated the use of plasmonic NPs for sensing adulterants and contaminants, however, these approaches often come with certain limitations. Han *et al.* fabricated p-nitroaniline (p-NA) functionalised AgNPs for the detection of melamine in infant formula. They achieved an LOD of 0.1 ppm [26]. Aquino *et al*. synthesized resorcinol-functionalized AuNPs for formaldehyde detection in an aqueous medium, where the NPs' colour changed blue from red in the presence of formaldehyde [27]. Teodoro *et al.* fabricated cellulose nanowhisker-functionalized AgNPs for hydrogen peroxide detection, achieving a LOD of 0.014 μM [28]. Aftab *et al.* synthesized selenium nanoparticles (SeNPs) for detection of salicylic acid in milk via colorimetric route, using garlic extract both as a stabilizing and reducing agent, achieving a LOD of 1 mM [29].

Gao *et al.* developed Triton X-100 modified AuNPs for smartphone-based system for melamine detection, which resulted in change in colour of NPs, with a LOD of 5.1 nM [30]. Mirzae *et al.* created sericin-capped AgNPs for detecting hydrogen peroxide in milk using an origami paper substrate, achieving a LOD of 44.1 μM [31]. Seebunrueng *et al.* designed a paper-based vapor-test kit, using coated filter paper, with a LOD of 3.66 μM for detection of formalin in food items [32]. Shrivas *et al.* reported AgNPs deposited on inkjet-printed paper for smartphone based on-site colorimetric determination of mercury ions (Hg^{2+}), with an LOD value of 49.9 nM [33]. Similarly, Wi *et al.* for fabricated a paper-based sensor foe detecting arsenic ions (As^{5+}) using methylene blue-AuNPs [34]. For detecting cadmium ions (Cd^{2+}) in rice samples Wang *et al.* developed a fluorescent based colorimetric paper strip with smartphone technology using ethylenediamine-graphene oxide (EDA-GO) and glutathione-gold nanoclusters (AuNCs), along with copper ions (Cu^{2+}). The LOD of the fabricated device was 0.1 μM [35]. In a study, Sahu *et al.* designed a dual paper-based sensor using glucose-AuNPs for sensing As^{3+} and lead ions (Pb^{2+}) in samples containing waste water with a LOD value of 74.7 nM and 37.2 nM, respectively [36].

Additionally, some studies have reported simultaneous detection of multiple adulterants in milk. Guinati *et al.* designed a paper-based detecting system for sensing H_2O_2, urea, and pH in raw milk samples. The LOD for urea and hydrogen peroxide were 2.4 mM and 0.1 mM, respectively [37]. Patari *et al.* fabricated another paper-based microfluidic sensor for detecting detergents, urea, salt, starch, soap, sodium hydrogen carbonate, and hydrogen peroxide achieving a LOD ranging between 0.05% (vol./vol.)-0.2% (vol./vol.) [38]. In all these cases, NPs were functionalized with agents responsible for binding the analyte of interest. This binding either changed the inter-particle distance or resulted in the oxidation of NPs, enabling the detection of milk adulterants and contaminants. However, these reported works used large amounts of toxic chemicals, making the detection schemes hazardous [39].

The goal of this chapter is to detect these adulterants via a less toxic, eco-friendly and cost-effective route that requires lesser detection time and displays higher recovery rate and sensitivity. This chapter focuses on the qualitative detection of adulterants by observing colorimetric changes upon the presence of the targeted adulterants and

contaminants. The first part of this chapter reports, *Camellia sinensis leaves extract*-functionalized AgNPs for interference-based colorimetric sensing of melamine in milk. *Bombax ceiba leaves extract*-functionalized AgNPs for sensing hydrogen peroxide in milk, where the colour changed from yellow to colourless. L-cysteine-functionalized AgNPs for sensing formalin in milk, with the colour changing from yellow to brown due to the aggregation of NPs in the presence of formalin. *Citrullus lanatus* rind extract-functionalized AgNPs were utilized for sensing salicylic acid in milk, with the colour changing from yellow to brown. Majority of the functionalizing agents are derived from natural sources, providing a less toxic route for the detection of milk adulterants. The UV-Vis response of these functionalized NPs was used to obtain a linear calibration graph, which helped determine the selectivity, sensitivity, recovery, and LOD.

Meanwhile, in the second part of this chapter, a novel paper-based sensing platform has been introduced, which uses multiple functionalized AgNPs for the simultaneous sensing of various contaminants and adulterants. This platform features seven conduits, each end selectively impregnated with specific functionalized NPs, separated by hydrophobic barriers. When adulterated or contaminated milk is poured at the centre, it flows through the channels and the resulting colour changes at the conduit ends indicate the presence of specific adulterants. This sensing architecture is specifically designed to detect melamine, formalin, and hydrogen peroxide as adulterants, and mercury, arsenic, cadmium, and lead ions as HM contaminants in milk, with each conduit achieving remarkably low detection limits, supplemented by high sensitivity.

2.2 Materials and methods

Fresh cow milk was procured from a local milk vendor. Processed green tea (GT) leaves were purchased from the Tezpur University market, Assam, India. Leaves from cotton tree (CT) were obtained from Jorhat, Assam, India. Watermelon Rind (WR) was procured from the Tezpur University market, Assam, India. Banana root bulb (BRB) was procured from nearby village area of Napaam, Tezpur, Assam, India. Silver nitrate and cyanuric acid were purchased from Thermo Fisher Scientific. Sodium borohydride ($NABH_4$), l-cysteine (l-cyst), polyvinyl alcohol (PVA), maleic acid (MA), l-glutamine (l-glu), citric acid (CA), trisodium citrate (TSC), salicylic acid (SA), dextrose and acidic buffer (pH 4) were from Merck, USA. Melamine (extra pure), urea (extra pure) and sodium hydroxide (NaOH)

pellets were procured from Loba Chemie. Trichloroacetic acid (TCA) was from Qualigens. Formaldehyde (37%) and hydrogen peroxide (30%) from Emplura. Sodium arsenite, cadmium chloride, mercury chloride, and lead chloride were also procured from Merck, USA. Whatman filter paper no. 1, 0.22 μm syringe filter, distilled water (DW), and deionized water (DI) were used for synthesis process.

Chromic acid and aqua regia (HNO_3: HCl; 1:3) were freshly prepared and were used for cleaning purpose. Ethanol, and acetone from Qualigens were also used for cleaning purposes.

2.3 Instruments

A UV−Visible spectrophotometer (Thermo Scientific GENESYS 180); an X-ray powder diffractometer (XRD) (D8 FOCUS, Bruker AXS, GERMANY& BRUKER D8 ADVANCE ECO); a Transmission electron microscope (TEM) (Tecnai G2 20 S-TWIN, USA); a Field emission scanning electron microscope (FESEM) (JEOL & GEMINI 500); a Fourier transform infrared spectroscopy (FTIR) (SPECTRUM 100, PerkinElmer); a weighing machine (METTLER TOLEDO ME204); a centrifuge machine (Eppendorf 5430R); an oven (Ecogian series; EQUITRON); a tabletop pH meter (EUTECH pH 700), and a magnetic stirrer (SPINOT-TARSONS) were also used during the work. A 3D printer was used to fabricate the platform to accommodate the paper-based substrate for colorimetric detection using ULTIMAKER S3 series printer.

PART A: Colorimetric sensing of milk adulterants without substrate

2.A.1 Colorimetric sensing of melamine by *Camellia sinensis* functionalised AgNPs*

Melamine, a highly toxic milk adulterant is often added to increase the non-protein nitrogen content of milk. Due to is texture and chemical nature, it's highly challenging to detect its presence in complex matrix such as milk. Hence, the current scenario demands a user-friendly detection measure for its sensing. Current techniques primarily describe sophisticated chromatographic techniques for melamine detection in milk, which require complex pretreatment procedures. Although some colorimetric methods exist, they also involve lengthy pretreatment and detection processes necessitating substantial chemical usage [16-20].

In contrast, our approach introduces an innovative, straightforward method for qualitatively assessing melamine levels in milk. This method leverages a direct greener compound for NP synthesis and subsequent detection of melamine without extracting bio-polyphenols from their sources. Unlike previous works that utilized chemical compounds unrelated to plant extracts, we emphasize using a greener agent for melamine detection. Our colorimetric detection method employs a one-pot sensing technique based on interference, where melamine disrupts NP formation. High melamine concentrations result in a colourless solution, while lower concentrations lead to the formation of larger, aggregated particles.

2.A.1.1 Synthesis of *Camellia sinensis* functionalised AgNPs and pretreatment of milk

Preparation of the Green Tea Extract: Processed green tea leaves were utilized for the synthesis process. Initially, 50 mL of DW was heated to 100°C in a 100 mL beaker for a duration of 15 min. Subsequently, 1 g of processed green tea leaves were introduced into the water and stirred using a glass rod. This tea mixture was kept aside for 15 min to allow release of all the antioxidants into the water. The extract prepared was then subjected to

* **This section of the thesis is published in U Das *et al. ACS Omega*, 9: 21879–21890, 2024**

double filtration using Whatman filter paper no. 1, which was then stored at 4 °C for later use [40].

Preparation of AgNPs: 1 mM $AgNO_3$ solution was prepared by adding 0.0169 g of $AgNO_3$ to 100 mL of DW. The solution was stirred for 15 min at a rate of 600 rpm to ensure complete dilution of the salt in the solution. Subsequently, 120 µL of green tea extract was introduced to $AgNO_3$ solution at room temperature while maintaining a pH of 7 by addition of NaOH. A change in colour of the solution to yellow signalled NP formation [40].

Pretreatment of milk: The presence of fat and protein in milk can cause potential interference with the detection mechanism, leading to erroneous results that may be either false positives or false negatives. However, this interference can be eliminated with the proper pretreatment of milk. To achieve this, fresh milk was initially treated by adding 50 mL of 10% trichloroacetic acid solution to 200 mL of milk in a 500 mL beaker. The resulting mixture was centrifuged twice, each time at 7000 rpm for 30 min, facilitating the separation of the protein and fat content. Subsequently, after successful separation of the solid casein and liquid supernatant, 3 M NaOH was introduced to the supernatant to adjust the pH of the solution to 7.0. The resulting supernatant was further subjected to dual filtration using Whatman no. 1 filter paper. The supernatant obtained at this stage was then filtered through a 0.22 µm filter to eliminate any residual protein and fat content remaining in milk. After following this process, the resultant milk supernatant, was then spiked with various concentrations of melamine (0.01 to 50 ppm) for subsequent testing [41].

2.A.1.2 Characterisation of *Camellia sinensis* leaves extract functionalised AgNPs

To affirm the formation of NPs, the synthesized NPs were first subjected to optical characterisation by using a standard UV−Vis spectrophotometer. This confirmation was based on the observation of an absorbance peak approximately at 418 nm which coincides with the LSPR band of plasmonic AgNPs. The synthesized NPs appeared yellow due to their reflection and scattering of yellow light, resulting from the absorption of blue light. This absorption aligns with the LSPR band position of AgNPs [42] (**Fig. 2.A.1.a**).

Furthermore, structural characterization of the synthesised NPs was accomplished through XRD study. Bragg diffraction peaks were obtained for diffraction planes (111), (200), (220), and (311) for 2θ values of 37.59º, 43.79º, 63.90º, and 76.94º, respectively, with the most intense diffraction peak occurring at the (111) plane. This diffraction pattern suggested that the synthesised NPs were face centred cubic (FCC) crystalline in nature [43] (**Fig. 2.A.1.b**).

Morphological parameters such as shape and size, were assessed through TEM and FESEM examinations. TEM data confirmed that the synthesized NPs exhibited a spherical shape with a mean diameter of 9.90 nm and size ranging between 5 and 20 nm [44] (**Fig. 2.A.1.c; Fig. 2.A.1.d** & **Fig. 2.A.1.e**). This was further corroborated by FESEM images, which also depicted that the synthesised AgNPs were mostly spherical in shape possessing an average size of 13.17 nm [45] (**Fig. 2.A.1.f**).

The FTIR method was employed for the comprehensive characterization of AgNPs, specifically focusing on identifying the functional groups responsible for the reduction, encapsulation and functionalisation of AgNPs. In the FTIR spectra of green tea, a notable broad band dip at 3395 cm^{-1} indicated the H-bonded OH stretch. Additional features included transmittance dips at 2920 and 2856 cm^{-1}, corresponding to the C−H stretch in alkanes and the O−H stretch in carboxylic groups, respectively. A distinct dip at 1635 cm^{-1} was attributed to the C=O stretch in polyphenols. Further dips at 1369, 1320, 1238, and 1149 cm^{-1} provided insights into the presence of carboxylic groups, aromatic nitro compounds, C≡C, and the secondary alcohol C−O stretch, respectively. The identification of C−O stretching in amino acids manifested as a dip at 1042 cm^{-1}. A weak transmittance dip at 824 cm^{-1} was associated with C−H out-of-plane bending, while peaks at 769, 611, and 522 cm^{-1} indicated the presence of aliphatic chloro and bromo compounds, signifying C−Cl and C−Br stretches. Comparing these results with those obtained for the green tea extract and the corresponding reduced NPs, significant dips were observed at positions 3434, 2920, and 2854 cm^{-1}. These indicated H bonded OH stretch, C−H stretch in alkanes, and O−H stretch caused by carboxylic acid, respectively. A highly intense transmittance dip at 1643 cm^{-1} can also be attributed to the C=O stretch in polyphenols and thus contributing to the functionalization of the NPs. Additionally, a transmittance dip at 1380 cm^{-1} affirmed the presence of methyl C–H asymmetric bending, collectively

confirming the proper functionalization of the NPs and the reduction of metals through the presence of these functional groups [46,47] (**Fig. 2.A.1.g**).

2.A.1.3 Colorimetric sensing

120 µL portion of green tea extract was combined with 400 µL of melamine spiked milk supernatant. The resulting solution underwent stirring at 600 rpm via a magnetic stirrer for 5 min. Subsequently, the solution's pH was adjusted to 7 by addition of NaOH, followed by addition of 10 mL of $AgNO_3$. The formation of NPs and the ensuing colorimetric changes in response to the melamine's concentration in spiked milk samples were subjected to further investigation by a standard UV−Vis spectrophotometer (**Fig. 2.A.2**).

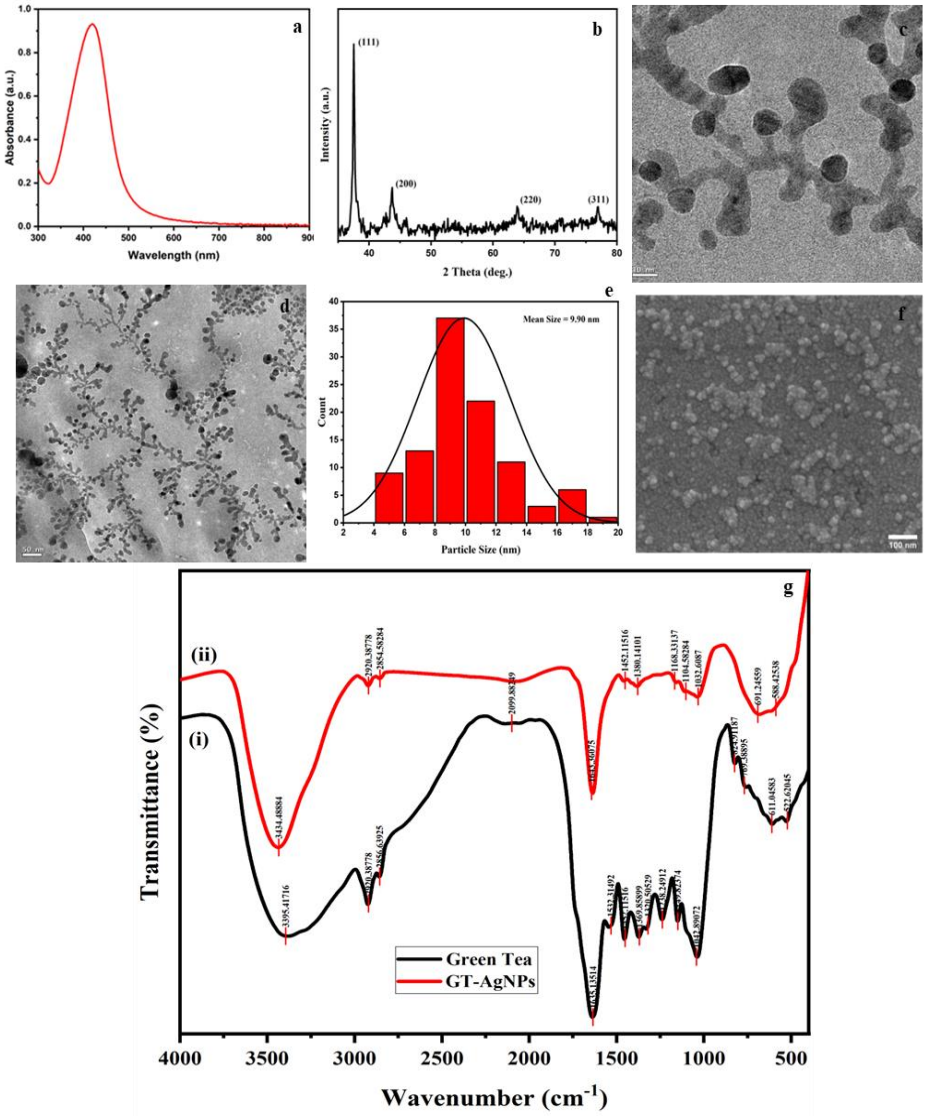

Figure 2.A.1: *Characterisation of GT-AgNPs* ***(a)*** *UV-Vis spectrum,* ***(b)*** *XRD pattern,* ***(c)*** *TEM image (high magnification),* ***(d)*** *TEM image (low magnification),* ***(e)*** *size distribution analysis from TEM,* ***(f)*** *FESEM image, and* ***(g)*** *FTIR spectrum.*

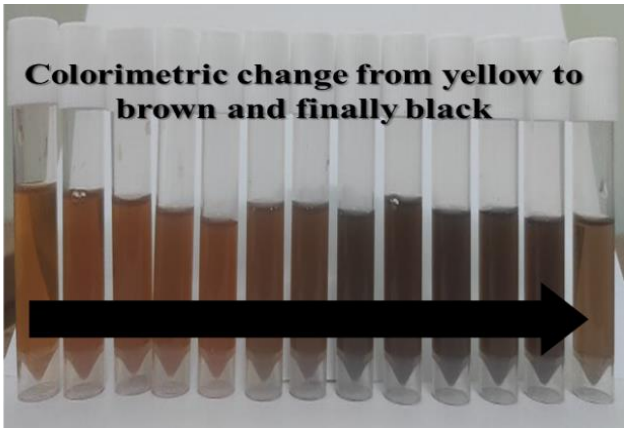

Figure 2.A.2: *Colorimetric change in GT-AgNPs at various concentration of melamine.*

2.A.1.3.1 Mechanism

This sensing protocol employs an eco-friendly material, green tea, which not only serves as a reducing agent by converting the metal ion (Ag^{+}) to NPs but also plays a pivotal role in detecting melamine. Green tea being an eco-friendly material mitigates any adverse environmental impacts. The phytochemicals present in green tea are responsible for reducing the ions to NPs but do not interfere with milk supernatant. This is due to the removal of interfering proteins and fats from the milk during a preprocessing step. In comparison with the previous reported works, where detection of melamine was performed by first NP synthesis followed by its complex functionalization for selective colorimetric sensing, our sensing approach takes a distinctive approach. [48,49] Green tea contains a diverse category of catechins, polyphenols responsible for melamine detection. These include (+)-catechin, (−)-epicatechin (EC), (+)-gallocatechin (GC), (−)-epicatechin gallate (ECG), (−)-epigallocatechin (EGC), and (−)-epigallocatechin gallate (EGCG) where primarily EGCG, is the dominant polyphenol in the green tea extract which encapsulated and functionalises the NPs [50]. However, in the presence of the melamine, plentiful polyphenol interacts with it, resulting in the formation of a compound that lacks any observable peak at that position. This implies that the extract can serve as an active agent for determining melamine in NPs [51].

In absence of melamine, the precursor and the green reducing agent i.e., green tea interact with each other. EGCG, being the most abundant polyphenol and antioxidant present in green tea, converts ions into NPs by reducing the silver ions present in the silver

precursor. As a result, bright yellow-coloured NPs solution could be obtained, which indicates formation of smaller sized NPs. However, in the presence of melamine, the three $-NH_2$ groups of melamine, interacts with the $-OH$ group of EGCG via hydrogen bonding. This interaction inhibits the formation of NPs as there are fewer available active sites for reducing the ions to particles, resulting in formation of larger aggregated particles. This suggests that polyphenols interacted with melamine instead of the silver ions (Ag^+) present in the solution. To study the reproducibility of the sensing method, the experiment was performed in triplicates, convergent findings were observed in all cases, demonstrating a uniform LOD and high repeatability [52].

In the presence of melamine, the reducing agent engages with it instead of the metal ions, resulting in the generation of fewer NPs or aggregated NPs of larger size with altered shapes [53,54]. This phenomenon results in colorimetric changes in the synthesized NPs, which could be correlated with the concentration of melamine in spiked milk. Melamine contains multiple hydrogen atoms, which enable strong interactions with the reducing agent [55] (**Fig. 2.A.3**).

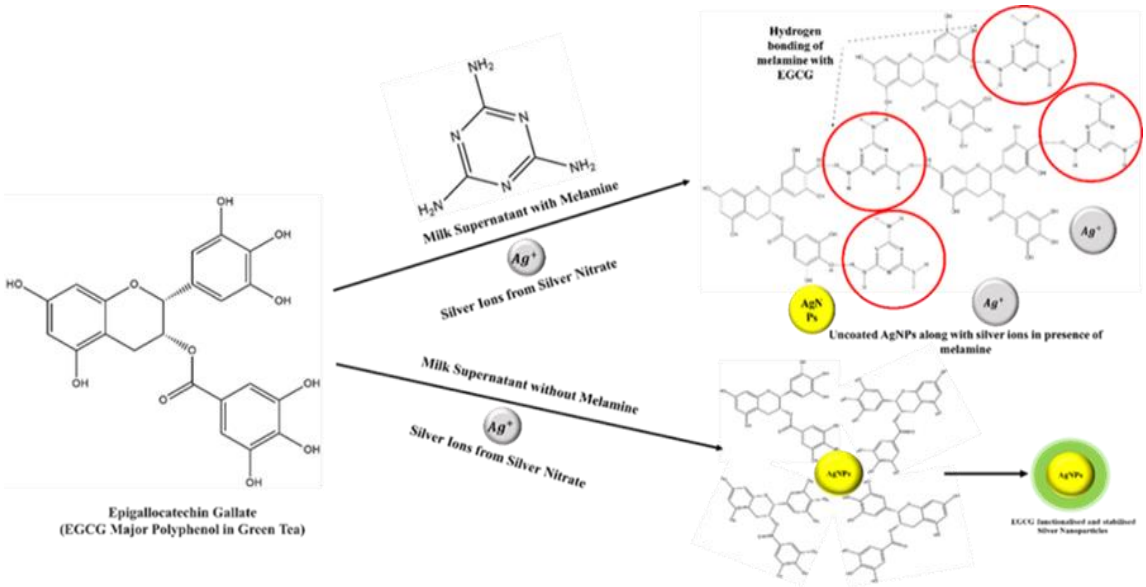

Figure 2.A.3: *Mechanism of melamine sensing by GT-AgNPs.*

2.A.1.3.2 Selectivity study

Green tea contains multiple flavonoids and bio polyphenols, which make it a strong antioxidant. However, presence of melamine, disrupts the formation of NPs. To ensure the

selectivity of the analysis and verify whether other potential adulterants or preservatives interfere with the sensing process, a comprehensive selectivity test was performed. For this assessment, milk samples were deliberately spiked with various adulterants such as formalin, urea, salicylic acid, dextrose, and cyanuric acid at a 1000 ppm concentration and melamine at 50 ppm concentration. The goal was to investigate whether the presence of other elements in trace amounts affects the detection process and also result in colorimetric change. The findings implied that none of these analytes significantly interfered with the synthesis of the NP prepared by the protocol. The colour of the salt solution changed to yellow or brown even in the presence of these adulterants, indicating no interference in formation of NPs by other adulterants. Therefore, the method is found to be appropriate for melamine detection without any observable interference from the reported adulterants [56] (**Fig. 2.A.4**).

2.A.1.3.3 Sensor performance metrics

To determine the LOD, a calibration graph was plotted correlating absorbance with the concentration of melamine. The colorimetric changes observed with increments in the concentration of melamine were analysed by a UV−Vis spectrophotometer, which revealed a substantial shift and decrease in absorbance. This can be attributed to a decrease in the number of NPs or the formation of larger-sized aggregated particles in the presence of melamine. Based on the response obtained from the UV−Vis spectrum, the LOD of the sensing scheme was calculated by using the slope (s) of the calibrated graph and the standard error (σ) (from 3 blank experiments) using the formula (**equation 2.A.1**) [57,58],

$$LOD = \frac{3.3\sigma}{s} \qquad (\mathbf{2.A.1})$$

The recovery rate was also accessed, which was found to be 93%. It was calculated by obtaining the theoretical amount of melamine added from the calibration graph and the amount of melamine added, by using the formula (**equation 2.A.2**) [58],

$$\text{Recovery} = \frac{Experimentally\ derived\ amount\ of\ melamine}{Actual\ amount\ of\ melamine} \text{ X } 100\% \qquad (\mathbf{2.A.2})$$

By analysing all the results, the LOD of the sensor was found to be 1.44 ppm which is much lower than the permissible limit suggested by FSSAI, limit of 2.5 ppm. The

sensitivity and dynamic range of sensing are also calculated from the calibrated graph. Sensitivity is determined by using the slope of the graph, yielding a value of 0.01 a.u./ppm (arbitrary unit/ppm). This sensitivity was achieved within a dynamic range spanning 0.1 to 15 ppm. Within this range, the sensor demonstrates a linear response in absorbance corresponding to changes in the melamine concentration in milk [59,60] (**Fig. 2.A.5**).

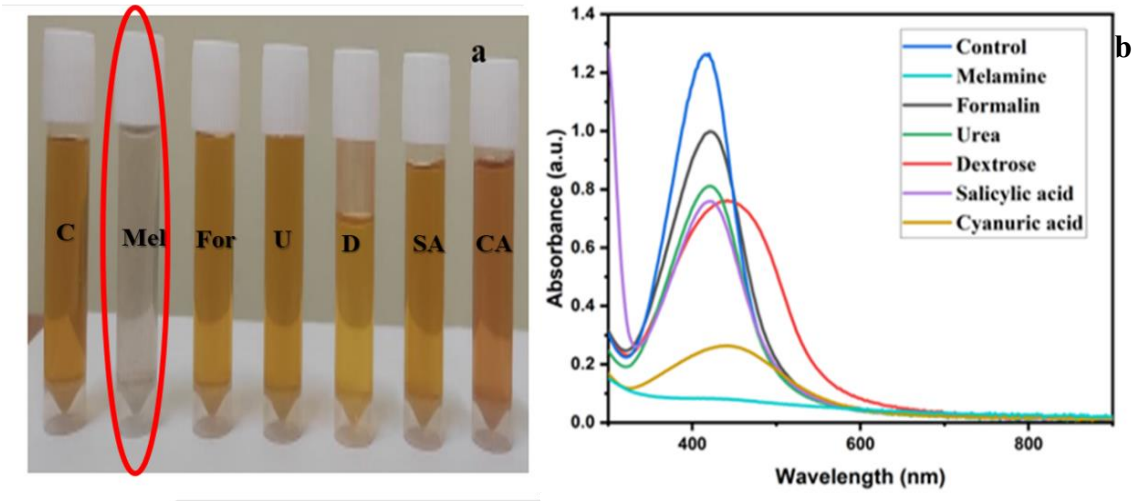

Figure 2.A.4: (a) *Colorimetric response of GT-AgNPs in the presence of various adulterants (C-Control, Mel-Melamine, For-Formalin, U-Urea, D-Dextrose, SA-Salicylic acid and CA-Cyanuric acid), and* ***(b)*** *UV-Vis plots of GT-AgNPs corresponding to their colorimetric variations in presence of other adulterants.*

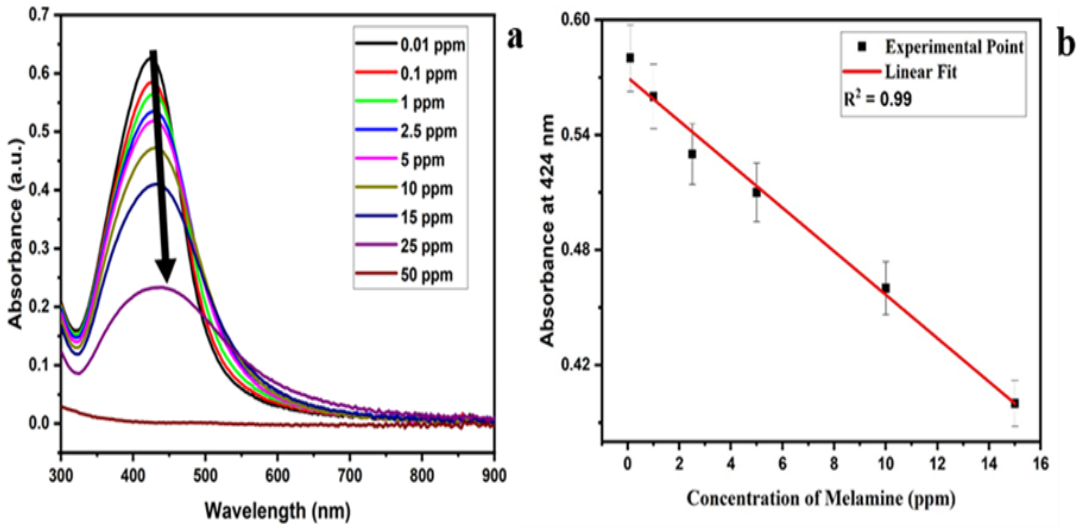

Figure 2.A.5: (a) *UV-Vis plot of synthesised GT-AgNPs in presence of melamine at varied concentration, and* ***(b)*** *linear calibrated graph between absorbance vs. concentration of melamine in milk.*

2.A.2 Colorimetric sensing of hydrogen peroxide by *Bombax ceiba* leaves functionalised AgNPs*

Hydrogen peroxide, a strong oxidizing agent, is often used as a milk adulterant to extend its shelf life by inhibiting the growth of microorganisms that cause spoilage. While it acts as an effective preservative, the consumption of hydrogen peroxide is highly toxic and poses serious health hazards, including irritation to the gastrointestinal tract, damage to tissues, and potential systemic toxicity at higher concentrations. Detecting hydrogen peroxide in milk is crucial to prevent its harmful effects [61].

AgNPs, known for their remarkable plasmonic properties, are widely used in colorimetric sensing applications. Traditionally AgNPs are synthesised and functionalised via physical or chemical route, which are not only expensive but also pose significant risks to human health, other living organisms, and the environment. In contrast, biosynthesised AgNPs offers a sustainable alternative, providing higher stability and yield. It can also be utilised as a highly efficient colorimetric sensor, which offers a rapid, simple, non-toxic, and eco-friendly, route enabling the production of NPs with well-defined sizes and reduced cytotoxicity [62].

The detection methods reported in the literature to sense hydrogen peroxide generally involves the use of spectrofluorometric, spectrophotometry, and electrochemistry [63]. Although these methods have revolutionized many fields, but they possess significant drawbacks including tedious sample preparation, expensive instrumentation, and time-consuming analysis. Therefore, an alternative method is needed to address these limitations and make the technology accessible for the use of common people. Few colorimetric methods have been documented in literature, but they often involve the use of harsh chemicals in NP synthesis, making it harmful for the environment [64]. Additionally, the synthesis procedure of these NPs is cumbersome and most of them do not target detection of this toxic compound in a complex matrix system like milk.

In contrast, our study introduces a streamlined and eco-friendly alternative where AgNPs were synthesized and functionalised using cotton leaf extracts. These biologically

* **This section of the thesis is published in U. Das *et al.*, *Spectrochimica Acta Part A: Molecular and Biomolecular Spectroscopy*, 316:124290, 2024**

derived NPs are utilized for the colorimetric sensing of hydrogen peroxide in milk. This method not only simplifies the detection process but also eliminates the need for complex preprocessing, making it a practical and sustainable solution for milk adulteration analysis.

2.A.2.1 Synthesis of *Bombax ceiba* leaves functionalised AgNPs and pretreatment of milk

Preparation of Bombax ceiba leaves extract: Cotton leaves were collected from a village area near Jorhat, Assam, India. These freshly collected leaves were then washed repeatedly with DI, chopped into small pieces and kept in an oven at 80ºC for 12 h for drying. 10 g of the dried leaves were added to a conical flask containing 100 mL of DW and boiled for 1 h at 100ºC. This extract solution was then allowed to cool down. Finally, it was double filtered through Whatman no. 1 filter paper and stored at 4ºC for further use [65].

Synthesis of AgNPs: At first, 1 mM $AgNO_3$ solution was prepared by adding 0.0169 g of $AgNO_3$ to 100 mL of DI which was stirred for 5 min and 600 rpm at room temperature to prepare the metallic salt precursor solution. To 40 mL of this solution, 400 µL of cotton leaves extract was added and stirred at 50ºC at 600 rpm. After 2 min, the solution exhibited a yellowish colour which indicated the formation of AgNPs. The entire synthesis was carried out at a pH of 7, which was maintained by adding NaOH to the colloidal solution [65].

Pre-treatment of milk: Same protocol was implemented as outlined in the previous study (section 2.A.1.1). After following this process, the resultant milk supernatant, was then spiked with various concentrations of hydrogen peroxide (1.5 to 30 ppm) for subsequent testing.

2.A.2.2 Characterisation of *Bombax ceiba* leaves extract functionalised AgNPs

Characterisation of the NPs were performed by following the previous protocol (section 2.A.1.2). UV–Vis spectra of the synthesised NPs displayed a strong absorption peak at 434 nm [42] (**Fig.2.A.6.a**).

In the XRD diffraction spectrum four distinct peaks were obtained at 2θ values of 37.82º, 45.82º, 64.15º and 76.34º which were attributed (111), (200), (220) and (311) planes of silver. This suggests that the synthesised AgNPs possess an FCC crystalline structure [43]. Further, two less intense diffraction peaks were also observed in the XRD diffractogram of the synthesised CT-AgNPs between 50° and 60°, it may have arisen from the minor phase impurities or lattice distortions introduced during synthesis. It can also be attributed to the presence of organic stabilizers or capping agents interacting with the NPs surface, which sometimes introduce additional diffraction peaks (**Fig.2.A.6.b**).

Images obtained from TEM analysis displayed roughly spherical and elongated structure with a mean size of 16.42 nm (**Fig.2.A.6.c; Fig.2.A.6.d.** & **Fig.2.A.6.e.**). [44]. Similarly, FESEM results depicted NPs of roughly spherical structure with some particles possessing an elongated shape having a mean size of 10.18 nm [45] (**Fig.2.A.6.f**).

For the functional group present in cotton leaves analysis, an FTIR study was conducted. A broad transmittance dip at 3430 cm^{-1} corresponds to the O–H stretching of hydrogen-bonded hydroxyl groups. Transmittance dips at 2953 cm^{-1} and 2914 cm^{-1} were attributed to the asymmetric and symmetric stretching vibrations of C–H bonds, typically from alkanes or alkyl groups. The absorbance peak at 1723 cm^{-1} corresponds to the stretching of the C=O group, indicated the presence of aldehydes, ketones, esters, or carboxylic acids, while the peak at 1622 cm^{-1} was associated with C=C stretching vibrations from alkenes or aromatic rings. Dips at 1406 cm^{-1} and 1378 cm^{-1} correspond to C–H bending vibrations from methyl or methylene groups, while dips at 1110 cm^{-1} and 1049 cm^{-1} were due to C–O or C–O–C stretching, commonly found in alcohols, ethers, or polysaccharides.

The FTIR spectrum of the NPs exhibited similar transmittance dips, suggesting the presence of comparable functional groups or chemical bonds to those in the reference material. For CT-AgNPs, a broad dip at 3430 cm^{-1} was observed, attributed to O–H stretching. Additional transmittance dips at 2922 cm^{-1} and 2852 cm^{-1} correspond to C–H stretching vibrations associated with alkyl groups. The dip at 1633 cm^{-1} indicates C=O stretching, while the dip at 1384 cm^{-1} corresponds to C–H bending, often linked to methyl groups or carboxylate ions. A dip at 1127 cm^{-1} was assigned to C–O stretching, likely from

alcohols, ethers, or esters. The similarity in transmittance dips between the FTIR spectra of the NPs and the cotton leaf extract suggests that the functional groups present in the NPs align closely with those in the extract. This indicates successful functionalization, the potential presence of stabilizing agents, and a comparable chemical composition between the two samples [66,67] (**Fig.2.A.6.g**).

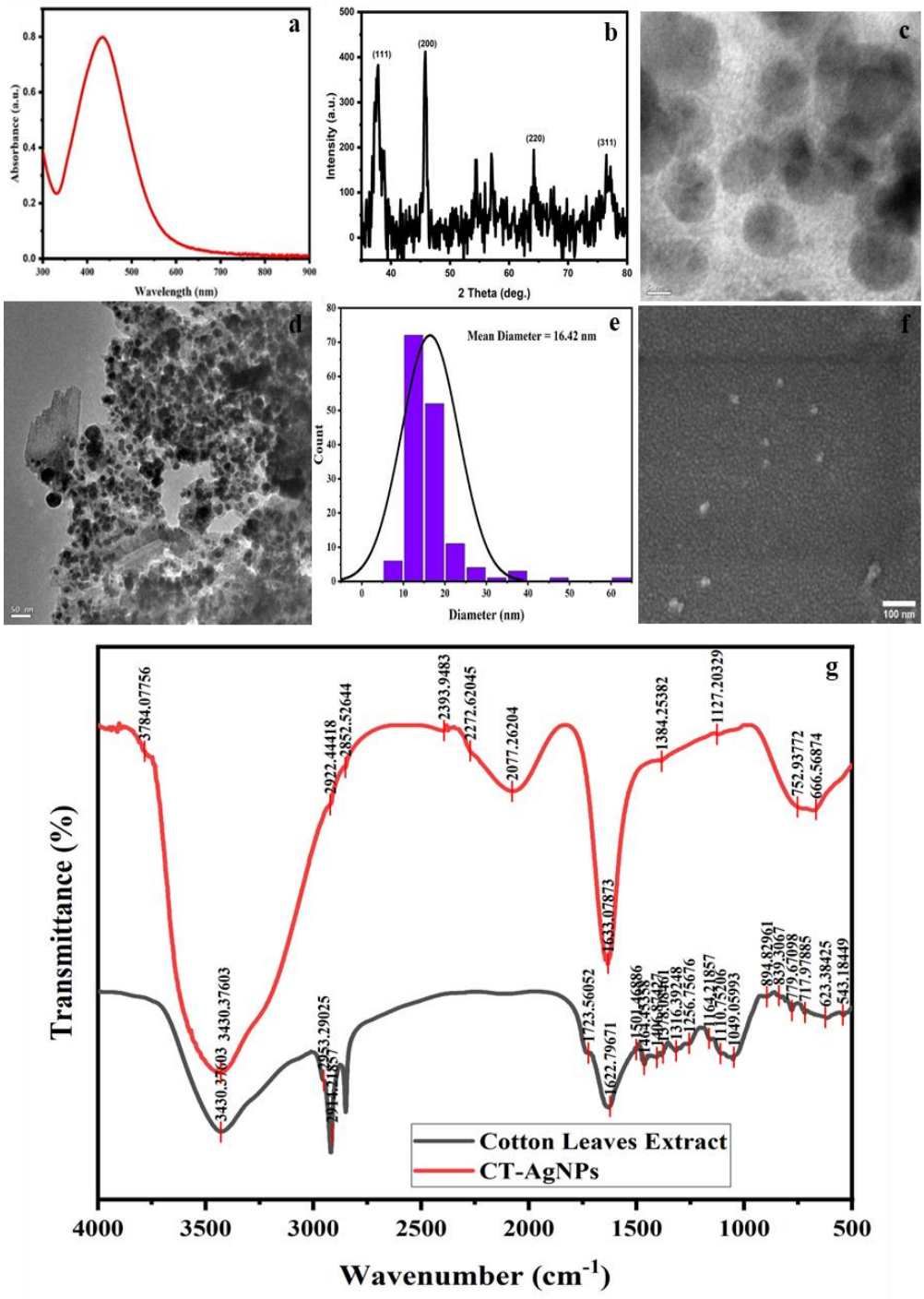

Figure 2.A.6: *Characterisation of CT-AgNPs* ***(a)*** *UV-Vis spectrum,* ***(b)*** *XRD pattern,* ***(c)*** *TEM image (high magnification),* ***(d)*** *TEM image (low magnification),* ***(e)*** *size distribution analysis from TEM,* ***(f)*** *FESEM image, and* ***(g)*** *FTIR spectrum.*

2.A.2.3 Colorimetric sensing

To perform the colorimetric detection, 400 µL of the H_2O_2 spiked milk supernatant of different concentrations (1.5 to 30 ppm) were added into 400 µL of AgNPs solution. Consequently, colour of the solution changed from yellow to light yellow and finally become colourless with increase in concentration of H_2O_2 in milk (**Fig. 2.A.7**).

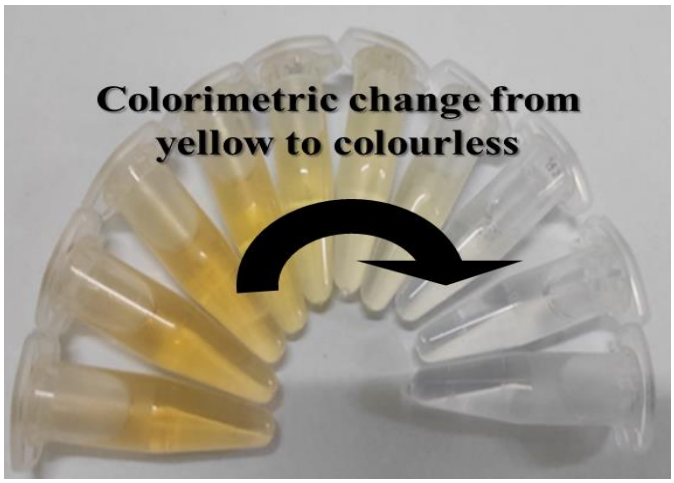

Figure 2.A.7: *Pictorial representation of colorimetric change of CT-AgNPs under various concentration of hydrogen peroxide.*

2.A.2.3.1 Mechanism

The antioxidant property of the cotton leaves extract not only facilitates reduction of Ag^+ to AgNPs but also provides a stable coating around the surface of the NP which prevents it from aggregating in presence of any other substance. But, the powerful oxidizing nature of hydrogen peroxide breaks the encapsulation of the functionalising agent and causes oxidation of AgNPs. This oxidation leads to the conversion of zero valent silver back to its ionic form. It results in formation of silver ions from NPs, leading to subsequent alteration of the colour of NP solution. As the concentration of hydrogen peroxide rises, the vulnerability of AgNPs to oxidation increases, resulting in a concurrent reduction of absorbance in the absorption spectra of the LSPR peak position due to a significant decline in the number of NPs present in the solution. As the standard potential of H_2O_2/H_2O ($E^0_{H_2O_2/H_2O}$ = 1.77 V) is higher than Ag^+/Ag ($E^0_{Ag^+/Ag}$ = 0.8V), in favourable medium the AgNPs get easily oxidised in presence of hydrogen peroxide (**Fig. 2.A.8**) [65,68-70].

2.A.2.3.2 Selectivity study

Cotton leaf extract is rich in antioxidants, which play a crucial role in reducing Ag^+ into AgNPs. Additionally, flavonoids and polysaccharides in the extract provide a unique encapsulation around the AgNPs, preventing their aggregation even in the presence of other chemicals. However, due to its strong oxidizing nature, hydrogen peroxide can oxidize the NPs. A selectivity study was also performed to determine the colorimetric changes in the synthesised NPs in presence of other adulterants such as formalin, salicylic acid, ammonium sulphate, urea and melamine in 100 ppm concentration each and hydrogen peroxide 20 ppm concentration in milk supernatant. It has been observed that there is no significant colorimetric change upon addition of different adulterant spiked milk to the NPs solution. There was also no significant decrease of shift in UV–Vis absorbance peak by addition of milk supernatant spiked with various interfering adulterants (**Fig. 2.A.9**).

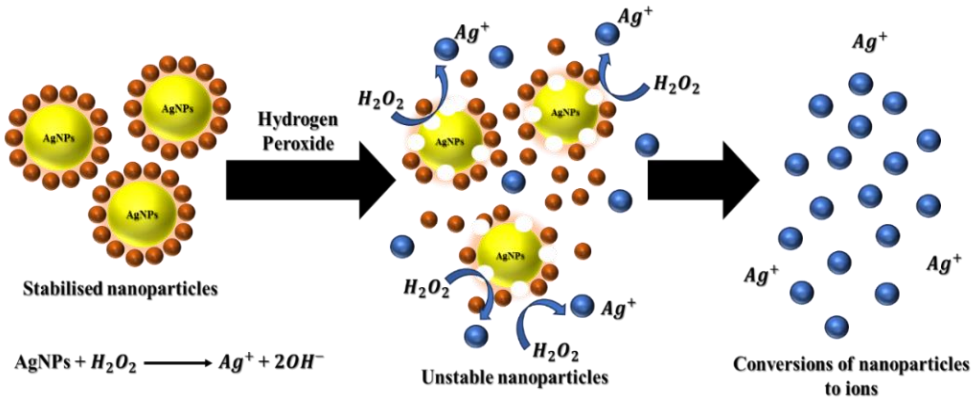

Figure 2.A.8: *Mechanism of sensing of hydrogen peroxide in milk.*

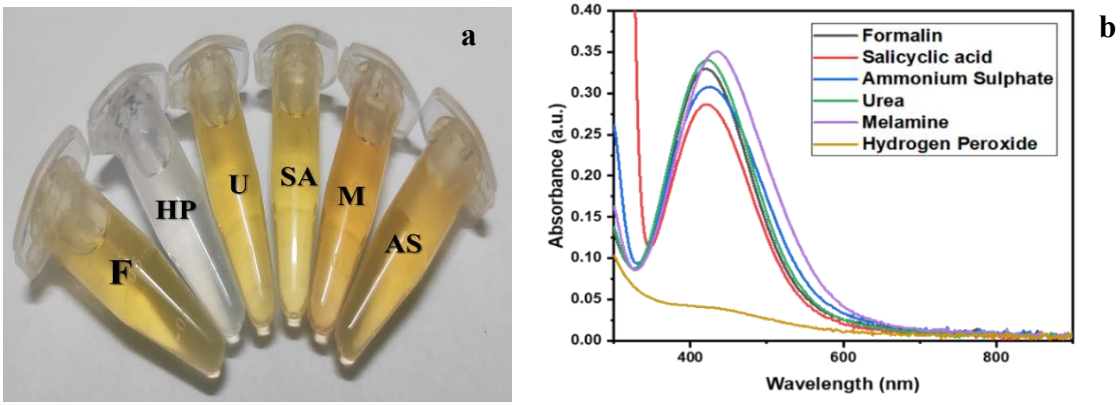

Figure 2.A.9: (a) *Colorimetric change in CT-AgNPs in presence of various adulterants (F-Formalin, HP-Hydrogen peroxide, U-Urea, SA-Salicylic acid, M-Melamine, and AS-Ammonium sulphate), and* ***(b)*** *UV-Vis plots of CT-AgNPs corresponding to their colorimetric variations in presence of various adulterants.*

2.A.2.3.3 Sensor performance metrics

To determine the LOD, of the sensor, the colorimetric variations was subjected to UV-Vis study. Where the colorimetric change in NPs indicated distinct spectral alterations corresponding to different concentrations of hydrogen peroxide. This highly efficient sensor can be utilised to qualitatively detect the levels of hydrogen peroxide concentration ensuring adherence to the its permitted limits in milk as defined by different countries which is deemed to be between 5–10 ppm. Significant decrease in absorbance was observed at 434 nm which can be attributed to the decrease in concentration of AgNPs with increase in hydrogen peroxide in milk [28,62,63].

From the UV-Vis spectra, a linear calibration graph was plotted between the absorbance at 434 nm of NPs against various concentration of the adulterant hydrogen peroxide (ranging from 1.5 ppm to 21 ppm) as they display a linear relationship with a R^2 value of 0.97. From the calibrated linear fitting graph, the standard deviation (of 3 blank measurements) and slope of the calibration graph were obtained which was then used in the standard formula for determination of LOD (as discussed in the previous section 2.A.1.3.3). The LOD was found to be 8.46 ppm. Similarly, by using the formula discussed in the previous chapter, the recovery rate of the sensing scheme was found to be 92% with a sensitivity of 0.03 a.u./ppm of hydrogen peroxide [65] (**Fig. 2.A.10**).

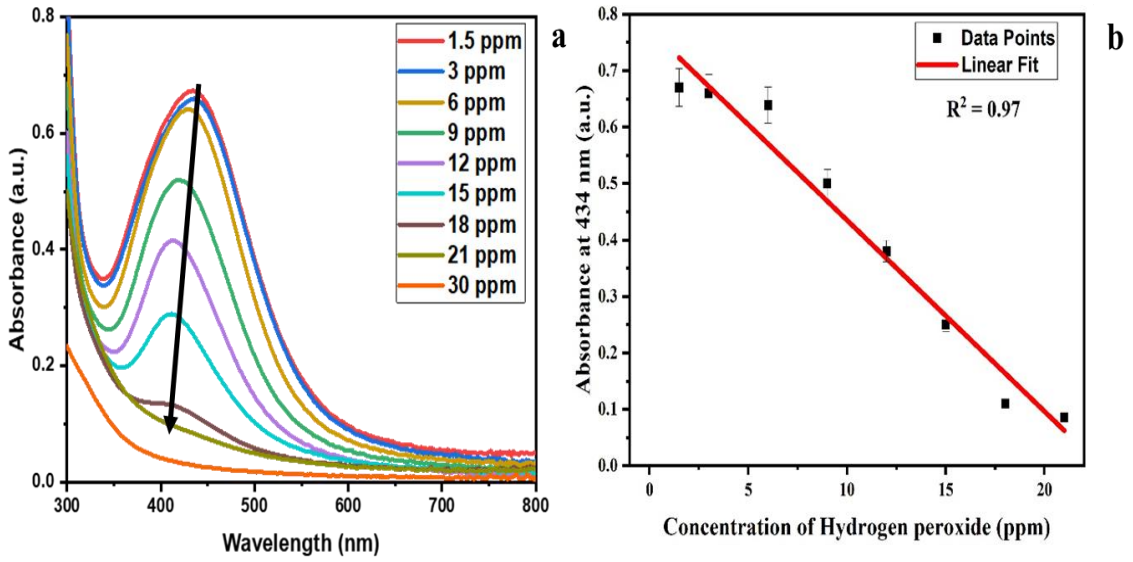

Figure 2.A.10: (a) *UV-Vis plot of the synthesised CT-AgNPs in presence of hydrogen peroxide in milk at varied concentration, and* ***(b)*** *linear calibrated plot between absorbance of NPs vs. concentration of hydrogen peroxide in milk.*

2.A.3 Colorimetric sensing of formalin by l-cysteine functionalised AgNPs

Milk is a perishable commodity that requires proper refrigeration to maintain its quality. Unscrupulous vendors may resort to using formalin as a cheaper alternative to refrigeration or other legal preservatives. While this might preserve the milk's appearance and delay souring, it poses significant health risks to consumers. It is toxic and carcinogenic to humans, and its consumption can lead to severe health consequences. Short-term exposure can cause abdominal pain, nausea, irritation of the gastrointestinal tract and vomiting, whereas. long-term consumption of may lead to chronic conditions such as cancer, respiratory problems, and kidney failure, as formaldehyde is a known carcinogen [71].

As it is a small volatile molecule, it can easily react with other substances, including milk proteins and fats [72]. Once the formaldehyde reacts, it may not remain in its free form, making it harder to detect directly. It can also form complexes with milk components, which can mask its presence. As a result, detecting formalin in milk is challenging, necessitating specialized pretreatment steps and the use of advanced instruments.

To address this gap, our study reports the detection of formalin as an adulterant using l-cysteine-functionalized AgNPs. Formalin exhibits a strong affinity for amino (-NH_2) groups. When it is introduced into the solution containing l-cysteine-functionalized AgNPs, it reacts with the amino groups on the l-cysteine. This chemical reaction primarily involves the formation of Schiff bases, altering the surface chemistry of the NPs. The interaction induces the aggregation of AgNPs by reducing the interparticle distance, which causes a distinct shift in their LSPR properties. This aggregation results in visible colour change, providing a straightforward and efficient means to detect formalin.

2.A.3.1 Synthesis of l-cysteine functionalised AgNPs and pretreatment of milk

Preparation of reducing and functionalising agents: 1 mM $AgNO_3$ solution was prepared by adding 0.0169 g in 100 mL of DW. For uniform dissolution of the precursor salt the

solution was stirred at room temperature for a duration of 10 min at a stirring rate of 600 rpm. Following which, 2mM of $NaBH_4$ solution was prepared by adding 0.008 g in 100 mL of DW for a duration of 5 min at room temperature at a stirring rate of 600 rpm. To properly cap and encapsulate the NPs 1% TSC solution was prepared for which 1 g of TSC was dissolved in 100 mL of DW at room temperature and a stirring rate of 600 rpm. For functionalisation of AgNPs, 2.8 mM l-cysteine solution was prepared for which 0.034 g of l-cysteine was added to 20 mL of DW solution and stirred at 60^oC for a duration of 30 min at a rate of 1000 rpm [73].

Preparation of AgNPs: To prepare the NPs, 28 mL of $NaBH_4$ was continuously stirred at 800 rpm, to it 14 mL of 1 mM $AgNO_3$ solution was added dropwise under continuous stirring to the solution. The colour of the solution immediately changed to yellow colour indicating formation of NPs in the solution. To prevent aggregation of particles 1 mL of TSC was added to this colloidal solution under continuous stirring at 800 rpm at room temperature. The stirring of NPs was continued for 20 min for uniform encapsulation and capping of each NP by the negatively charged citrate group. Following this 0.5 mL of 2.8 mM l-cysteine solution was added to the synthesised NP solution which was then stirred at 900 rpm for 15 min at room temperature for uniform surface functionalisation of the citrate capped NPs with l-cysteine. The pH of the solution was then adjusted to 7 by adding 0.1 M NaOH solution under continuous stirring at 900 rpm. The resulting solution was greenish yellow in colour indicating formation of l-cysteine functionalised AgNPs [73].

Pretreatment of milk: Same protocol was implemented as outlined in the previous study (section 2.A.1.1). After following this process, the resultant milk supernatant, was then spiked with various concentrations of formalin (0.1 to 100 ppm) for subsequent testing.

2.A.3.2 Characterisation of l-cysteine functionalised AgNPs

Characterisation of the NPs were performed by following the previous protocol (section 2.A.1.2). UV–Visible analysis was performed where the NPs displayed a sharp absorption peak at 391 nm. Occurrence of this sharp peak confirms formation of less polydisperse and smaller sized AgNPs in the solution (**Fig. 2.A.11.a**) [42].

To determine the crystallographic structural study of the synthesised NPs, XRD analysis was performed. From XRD, four distinct peaks were obtained at 2θ values of 37.53º, 43.82º, 63.98º and 76.96º in the XRD diffractogram which is attributed (111), (200), (220) and (311) planes of silver. This suggests that the synthesised AgNPs possess an FCC crystalline structure (**Fig. 2.A.11.b**) [43].

Images obtained from TEM analysis of synthesized NPs displayed is roughly spherical structure and were of a mean size of 10.85 nm [44] (**Fig. 2.A.11.c; Fig. 2.A.11.d** & **Fig. 2.A.11.e**). Similarly, FESEM images obtained from the analysis mostly depicted NPs of mean diameter of 11.47 nm which are roughly spherical structure (**Fig. 2.A.11.f**) [45].

FTIR characterization was performed to identify the functional groups responsible for the encapsulation and functionalization of NPs. The FTIR spectrum of l-cysteine revealed characteristic transmittance dips, including a broad dip at 3436 cm^{-1} attributed to O–H or N–H stretching vibrations, which likely arise from hydroxyl groups (O–H) in carboxylic acids or amino groups (N–H) in the molecule. Additional dips at 2982 cm^{-1} and 2083 cm^{-1} correspond to C–H stretching vibrations from alkyl groups or methylene ($-CH_2$) groups, while the dip at 2542 cm^{-1} represents the S–H stretching vibration characteristic of the thiol (-SH) group. The absorption band near 1600–1650 cm^{-1} may be attributed to presence of C=C stretching vibrations in alkenes, C=C stretching in aromatic rings. Additionally, the bands between 1406 and 1197 cm^{-1} correspond to C–H stretching or C–O stretching, common in amino acid structures.

In the FTIR spectrum of l-cysteine-functionalized NPs, dips observed at 3428 cm^{-1}, 2089 cm^{-1}, 1631 cm^{-1}, and 1388 cm^{-1} confirm successful functionalization. The dip at 3428 cm^{-1} corresponds to O–H or N–H stretching vibrations, indicating the presence of hydroxyl (-OH) or amine ($-NH_2$) groups that likely interact with the NP surface via hydrogen bonding. The dip at 2089 cm^{-1} suggests weak C≡N stretching or S–H stretching, representing interactions of the thiol (-SH) group, a crucial functional group for binding to AgNPs. The dip at 1631 cm^{-1} is attributed to C=O stretching vibrations from the carboxyl (-COOH) group or N–H bending, highlighting the involvement of carboxylic or amine groups in coordinating with the NP surface. The dip at 1388 cm^{-1} may corresponds to C–

H bending or symmetric COO^- stretching from deprotonated carboxyl groups (**Fig. 2.A.11.g**) [73,74].

2.A.3.3 Colorimetric sensing

0.5 mL of formalin-contaminated milk supernatant is added to 1 mL of l-cysteine-functionalized AgNPs (**Fig. 2.A.12**). Upon its addition the colour of the NPs changes from greenish yellow to orange and finally dark brown with increase in concentration of formalin.

2.A.3.3.1 Mechanism

For detecting formalin, AgNPs are surface-functionalized with l-cysteine. The functionalization involves strong binding between the thiol (-SH) group of l-cysteine and the AgNPs surface, forming a stable NP-ligand complex. When formaldehyde is introduced, it reacts primarily with the amine ($-NH_2$) group of l-cysteine, leading to the formation of Schiff bases formaldehyde-derived products. This interaction alters the surface properties and aggregation behaviour of the NPs [75].

The interaction between formaldehyde and l-cysteine-functionalized AgNPs reduces the interparticle distance, due to changes in the surface charge or chemical cross-linking facilitated by formaldehyde. This reduction in interparticle distance causes a shift in the LSPR of the AgNPs, resulting in a visible colour change. The NP solution transitions from greenish-yellow to brown or black as aggregation progresses. This colorimetric shift serves as a direct and visual indicator of formalin presence in formalin-adulterated milk. [75,76] (**Fig. 2.A.13**).

2.A.3.3.2 Selectivity study

A selectivity study was also performed to determine the colorimetric changes in the synthesised NPs in presence of other common milk adulterants such as melamine, hydrogen peroxide, urea, and dextrose in 100 ppm concentration and formalin in 20 ppm concentration. It has been observed that there is no significant colorimetric change or decrease/shift in UV–Vis absorbance peak upon addition of different adulterant spiked

milk to the NPs solution. This is due to the fact that L-cysteine on the surface of AgNPs selectively binds with formalin which results in aggregation of NPs (**Fig. 2.A.14**).

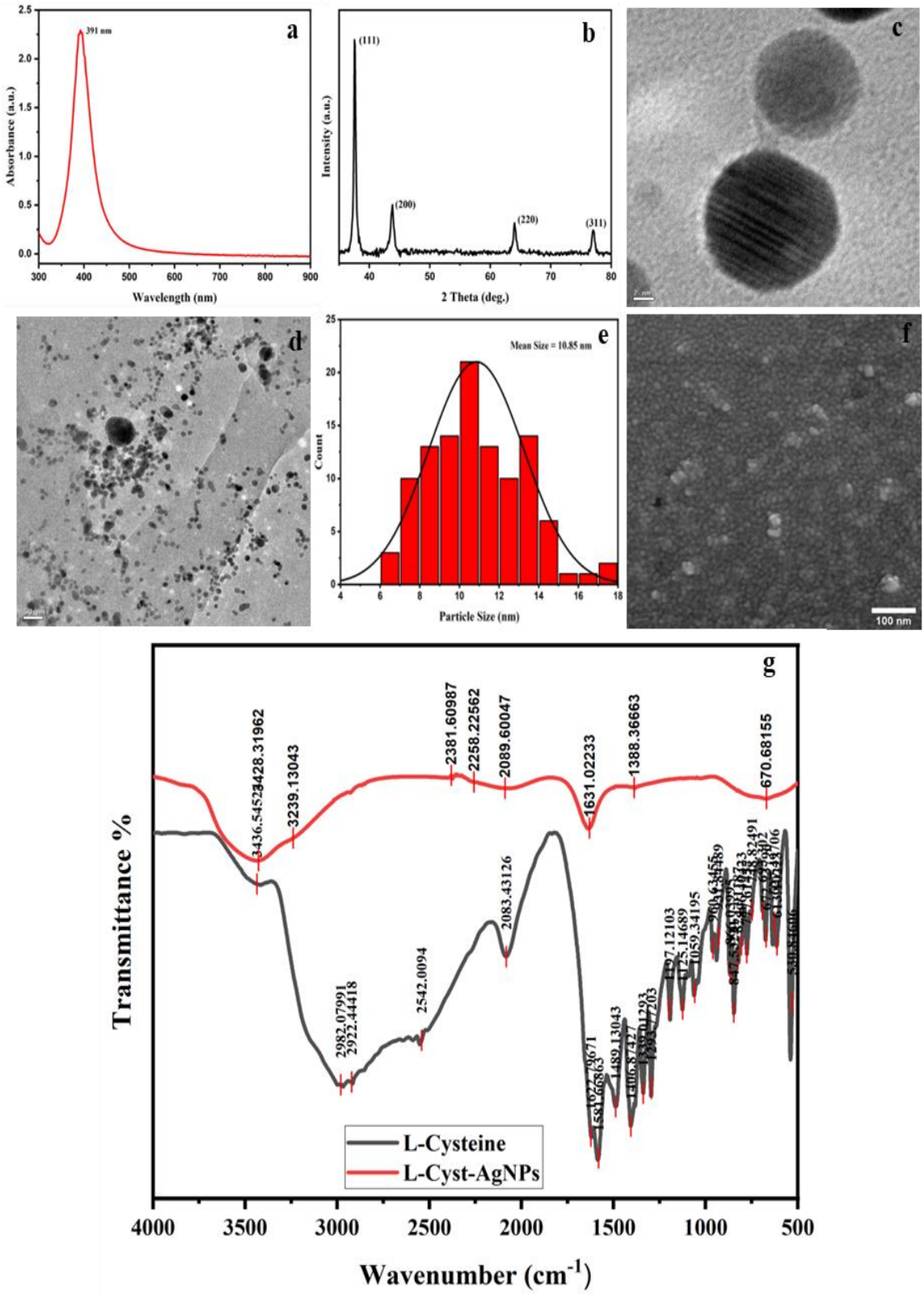

Figure 2.A.11: *Characterisation of l-cysteine-AgNPs* ***(a)*** *UV-Vis spectrum,* ***(b)*** *XRD pattern,* ***(c)*** *TEM image (high magnification),* ***(d)*** *TEM image (low magnification),* ***(e)*** *size distribution analysis from TEM,* ***(f)*** *FESEM image, and* ***(g)*** *FTIR spectrum.*

Figure 2.A.12: *Pictorial representation of colorimetric change of l-cysteine-AgNPs under various concentration of formalin.*

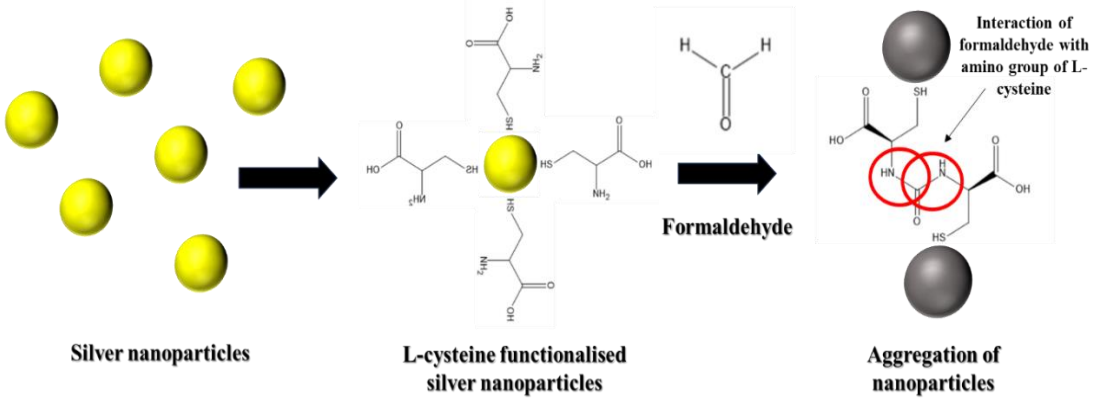

Figure 2.A.13*: Mechanism of colorimetric sensing of formalin by l-cysteine-AgNPs.*

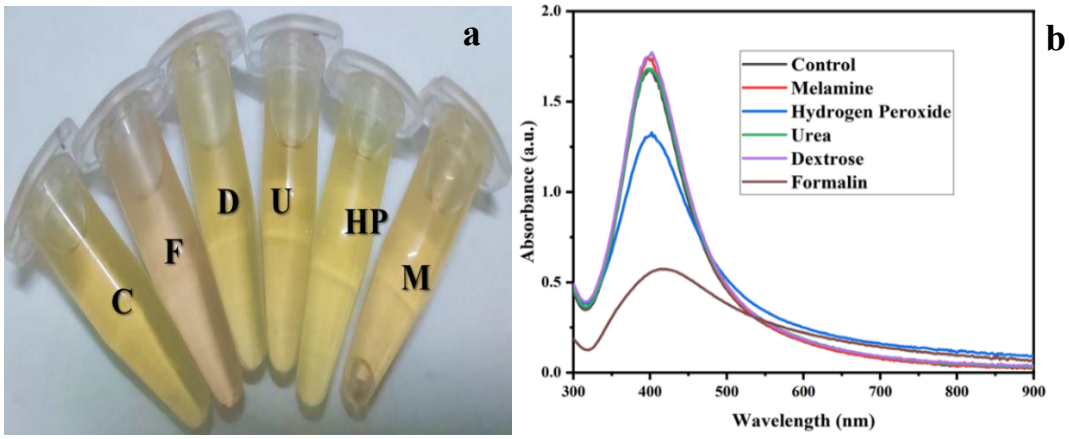

Figure 2.A.14: *(a) Colorimetric change in l-cysteine-AgNPs (C-Control, F-Formalin, D-Dextrose, U-Urea, HP-Hydrogen peroxide, and M-Melamine) and (b) UV-Vis plots of NPs corresponding to their colorimetric variations in presence of various adulterants.*

2.A.3.3.3 Sensor performance metrics

The LOD for formalin is determined by analysing the UV-Vis data, where the absorbance ratio of the NPs is measured in response to varying concentrations of formalin in milk. A calibration graph was then plotted, showing the relationship between the absorbance ratio

and the concentration of formalin. As there has been a significant decrease in absorbance at 394 nm and increase in absorbance at 500 nm caused by aggregation of particles. Regression analysis was performed on this calibration graph to obtain the slope and standard deviation, which are used to calculate the LOD (by using the formula reported in the previous study), found to be 3.51 ppm, with a recovery rate of 90% and a sensitivity of 0.002 change in absorbance ratio/ppm (**Fig.2.A.15**) [77].

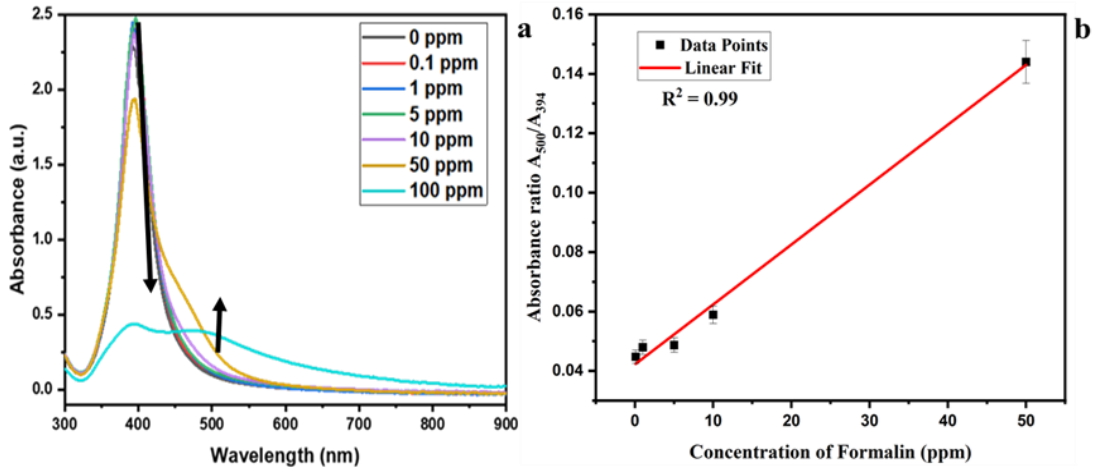

Figure 2.A.15: (a) *UV-Vis plot of the synthesised l-cysteine-AgNPs in presence of formalin in milk at varied concentration, and* ***(b)*** *linear calibrated graph between absorbance ratio vs. concentration of formalin in milk.*

2.A.4 Colorimetric sensing of salicylic acid by *Citrullus lanatus* rind functionalised silver nanoparticles*

Salicylic acid, a commonly used preservative, is a significant milk adulterant added to extend the shelf life of milk, typically at concentrations of 0.04–0.05%. Despite its widespread use, salicylic acid poses severe health risks, including gastrointestinal irritation, organ damage, and potential long-term toxicity, leading to its regulatory ban in many countries. However, deliberate adulteration with salicylic acid remains prevalent. Detecting this adulterant is essential to ensure milk safety and prevent associated health hazards [78].

Plasmonic NPs, particularly AgNPs, offer an innovative approach to adulterant detection due to their exceptional optical properties. When exposed to adulterants, AgNPs undergo a shift in their LSPR band, leading to detectable changes in the optical properties,

*This section of the thesis is published in U Das *et al.*, *Measurement*, 242: 115818, 2025

including colour variation. This principle has been effectively utilized in the fabrication of colorimetric sensors, enabling rapid, sensitive, and straightforward detection of milk adulterants [79].

Traditionally, AgNPs are synthesized through chemical or physical routes, while effective, are often expensive and harmful to both human health and the environment. In contrast, biosynthesized AgNPs, using plant extracts or other biological reducing agents, provide an eco-friendly, cost-effective alternative. These biosynthesized NPs exhibit excellent stability and high sensitivity, making them suitable for practical applications. The combination of these features highlights the potential of AgNPs as a reliable and accessible solution for ensuring the quality and safety of dairy products while minimizing environmental and health impacts.

So far, only one study by Aftab *et al.* has reported detection of salicylic acid in milk by using selenium NPs with a detection limit of 10^{-3} M [29].

Taking cue from this, the current study uses biogenic AgNPs from watermelon rind extract to create plasmonic AgNPs for colorimetric sensing of salicylic acid in milk. Compared to previous studies, this detection method is more robust, simple, and cost-effective, paving way for a novel, eco-friendly approach for detecting salicylic acid. The method demonstrated a low LOD and higher recovery rates than those reported in existing literature.

2.A.4.1 Synthesis of *Citrullus lanatus* rind functionalised AgNPs and pretreatment of milk

***Preparation of Watermelon Rind Extract*:** The outer green peel of the watermelon was removed carefully, and the white rind part was collected. The white rind was then chopped into small parts and subjected to drying in an oven at 100°C for 8 h. Once dried, they were then thoroughly washed with DW multiple times. Subsequently, 40 g of the dried rind was added to conical flask containing 100 mL of DW. This solution was then heated at 100°C for 1 h. Afterward, the extract was double-filtered twice using Whatman filter paper no. 1 to remove any impurities. The filtered extract was then stored at 4°C for further use [80].

Synthesis of AgNPs: To prepare a 1 mM $AgNO_3$ solution, 0.0169 g of $AgNO_3$ was added to 100 mL of DW and dissolved under magnetic stirrer for 5 min at 600 rpm. Subsequently, 20 mL of this $AgNO_3$ was stirred continuously at 60°C at 700 rpm. To this solution, 800 µL of WR extract was introduced and was stirred for 20 min at 60°C at 600 rpm. The colour of the solution changed to yellow, indicating the synthesis of NPs. Finally, the pH of the NP solution was brought to 7 by adding NaOH [80].

Pretreatment of Milk: Same protocol was implemented as outlined in the previous study (section 2.A.1.1). After which, the resultant milk supernatant, was then spiked with various concentrations of salicylic acid (0.05 to 15 ppm) for subsequent testing.

2.A.4.2 Characterisation of *Citrullus lanatus* rind functionalised AgNPs

Characterisations of the functionalised NPs were performed by using the methodology as reported in the previous sections. The UV-Vis spectrophotometer, revealed a distinct LSPR peak at 395 nm. This indicated the formation of less polydisperse NPs of very small size (**Fig. 2.A.16.a**) [42].

The XRD diffraction pattern of the synthesized NPs displayed four distinct peaks, indicating that the synthesised NPs are crystalline in nature. These peaks corresponded to the (111), (200), (220), and (311) crystallographic planes, with 2θ values of 38.18°, 44.4°, 64.51°, and 77.41°, respectively. The occurrence of these specific diffraction peaks suggests that the synthesized NPs exhibit an FCC structure (**Fig. 2.A.16.b**) [43].

TEM images depicted that the synthesised NPs were spherical and some of them are hexagonal in shape. The size distribution profile displayed that the NPs ranged from 1 to 30 nm, with an average diameter of approximately 12.07 nm (**Fig. 2.A.16.c; Fig. 2.A.16.d** & **Fig. 2.A.16.e**). Additionally, FESEM examination was also performed which also displayed same results (**Fig. 2.A.16.f**) [44]**.**

To determine the functional groups responsible for functionalisation, reducing and encapsulation of NPs, FTIR characterisation was performed. The spectra revealed a significant transmittance dip around 3450 cm^{-1}, corresponding to the hydroxyl group (H-bonded OH stretch) indicative of the OH stretch of water molecules in the rind extract.

This hydroxyl group was also involved in the functionalization of the NPs. Peaks at 1734 and 1637 cm^{-1} correspond to the C=O stretching of esterified carboxylic groups (-$COOCH_3$) and free carboxylic groups (-COOH), respectively. The symmetric vibrations of ionic carboxylic groups (–COO−) appear at 1489 and 1447 cm^{-1}. The peak at 1394 cm^{-1} has been assigned to the symmetric stretching of pectin, and the peaks from 1350 to 1000 cm^{-1} are attributed to the stretching vibrations of carboxylic acids and alcohols. The FTIR spectrum of the watermelon rind extract indicates the abundant presence of carboxylic and hydroxyl groups, which act as proton donors for binding cations. These functional groups facilitate the functionalization of the NPs, as evidenced by similar transmittance dips observed in the NPs themselves (**Fig. 2.A.16.g**) [81].

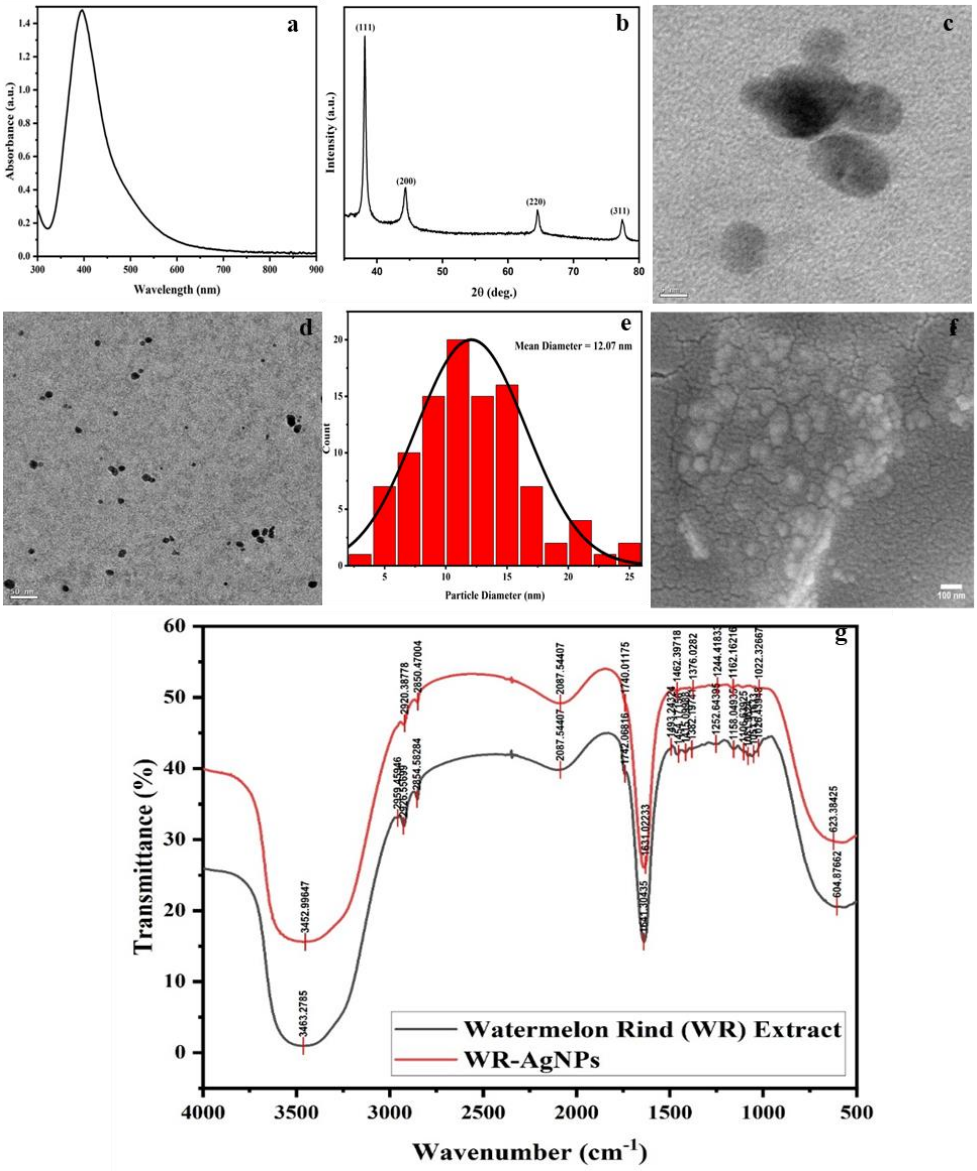

Figure 2.A.16: *Characterisation of WR-AgNPs* ***(a)*** *UV-Vis spectrum,* ***(b)*** *XRD pattern,* ***(c)*** *TEM image (high magnification),* ***(d)*** *TEM image (low magnification),* ***(e)*** *size distribution analysis from TEM,* ***(f)*** *FESEM image, and* ***(g)*** *FTIR spectrum.*

2.A.4.3 Colorimetric sensing

1 mL of the salicylic acid-spiked milk supernatant at various concentration (0.05 to 15 ppm) was introduced to 3 mL of the WR-AgNPs solution and incubated for 30 min at ambient temperature (**Fig. 2.A.17**).

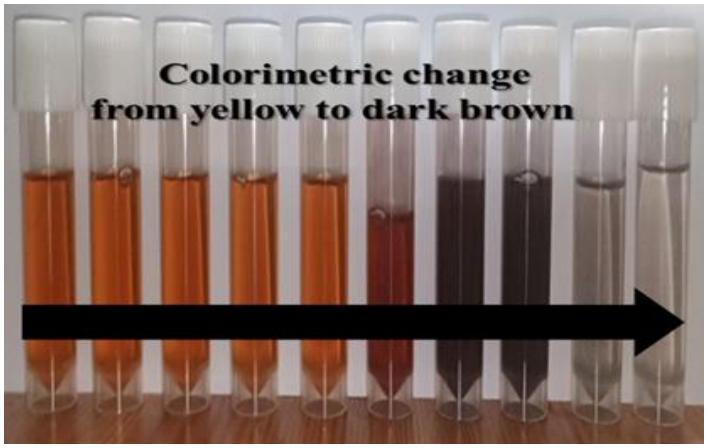

Figure 2.A.17: *Pictorial representation of colorimetric change of WR-AgNPs under various concentration of salicylic acid.*

2.A.4.3.1. Mechanism

Colorimetric sensing leverages the principle of induced NP aggregation in presence of an analyte. In this work, watermelon rind extract was used as a functionalizing agent for synthesizing NPs. Due to its abundant antioxidants, it possesses, excellent reducing property and helps in reduction of metal ions to NPs. The antioxidants in the watermelon rind extract provide a source of electrons which helps in conversion of Ag^{+} to zerovalent silver, which then agglomerates into NPs of the desired size. This synthesis approach is commonly referred to as the bottom-up method [82].

FTIR analysis revealed that watermelon rind is rich in carboxylic and hydroxyl groups, which act as proton donors for binding cations. Additionally, the rind contains high levels of vitamin C, dietary fiber, citrulline, potassium, and small amounts of vitamin B-6. These components not only help in reduction of Ag^{+} to NPs but also helps in surface functionalization of the NPs-enhancing their selectivity. This functionalization enables specific interactions with salicylic acid in milk, as salicylic acid contains two OH groups that can engage in hydrogen bonding with other OH groups present in the watermelon rind extract, particularly those from vitamin C. The FTIR spectra confirmed the presence of

these hydroxyl groups on the functionalized NPs. The hydrogen bonding between the OH groups of the NPs and salicylic acid reduce the interparticle distance, leading to NP aggregation [81-83].

The agglomeration of NPs causes a colorimetric change, which is evidenced by a prominent decrease and shift in the LSPR peak. This shift confirms the interaction and subsequent agglomeration of the NPs, validating the presence of salicylic acid in the sample [84] (**Fig. 2.A.18**).

2.A.4.3.2. Selectivity study

Selectivity analysis was conducted to assess the potential interference caused by other common adulterants in milk. The study evaluated the presence of substances such as melamine, urea, and formalin in 75 ppm concentration and salicylic acid in 15 ppm concentration in milk supernatant to determine their impact on the absorbance of the sensing scheme. The results displayed that there was no significant decrease or shift in absorbance when these other adulterants were present. In contrast, only the presence of salicylic acid resulted in a pronounced decrease in absorbance. This distinct response indicates that the fabricated sensing scheme is highly selective and effective for detecting salicylic acid in milk. The high selectivity underscores the robustness and reliability of the method, ensuring that it can accurately identify salicylic acid without being confounded by other potential adulterants (**Fig. 2.A.19**).

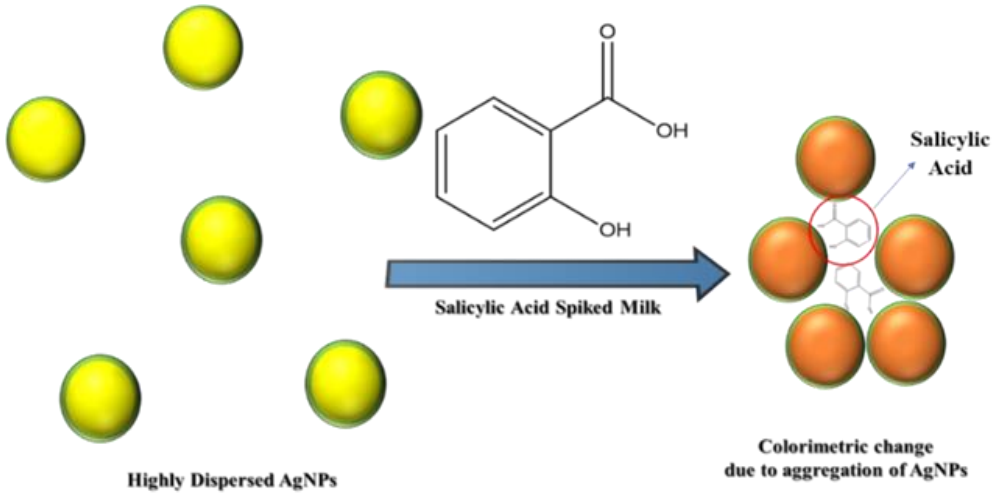

Figure 2.A.18: *Mechanism for colorimetric sensing of salicylic acid by WR-AgNPs.*

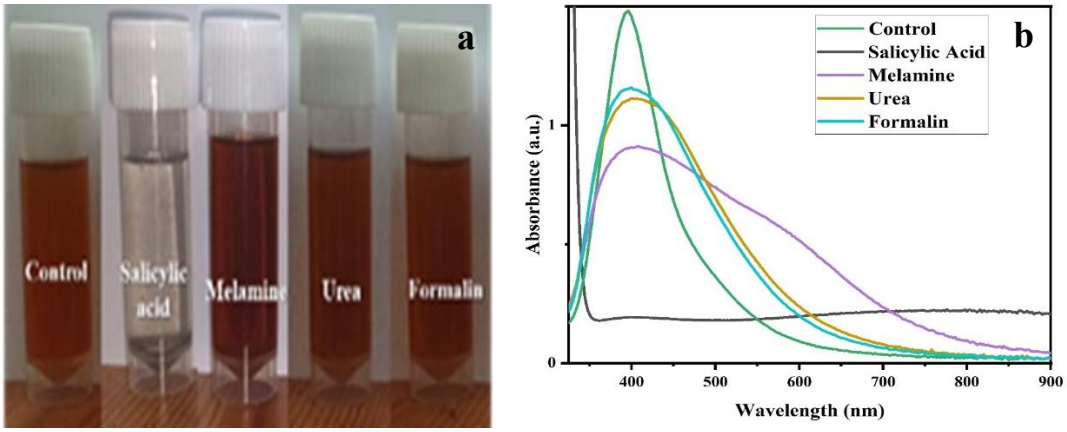

Figure 2.A.19: (a) *Colorimetric change in NPs in presence of other adulterants (Control, Salicylic acid, Melamine, Urea, and Formalin), and* ***(b)*** *UV-Vis plots of NPs corresponding to their colorimetric variations.*

2.A.4.3.3 Sensor performance metrics

The visible colorimetric change observed in the images was validated and quantified using UV-Vis spectroscopy. In the UV-Vis spectra, a significant decrease in absorbance was observed at the LSPR peak position of 395 nm. This peak is characteristic of AgNPs indicating their presence and specific optical properties. Concurrently, an increase in absorbance was noted at 551 nm, which is indicative of NP aggregation. This aggregation occurs due to the reduction in interparticle distance, which is caused by presence of analyte salicylic acid. To further analyse this phenomenon, a calibration graph was plotted between the absorbance ratio (A_{551}/A_{395}) and the concentration of salicylic acid in milk. The resulting linear trend depicted an increment in the absorbance ratio with rising concentrations of salicylic acid. This is due to the fact that higher concentrations of salicylic acid induce greater aggregation of NPs, thereby reducing their interparticle distance. The linearity of this trend is crucial for qualitative analysis, providing a reliable method for determining salicylic acid concentrations in adulterated milk samples [85].

In general, NP aggregation alters the optical properties due to changes in their size and shape. This is reflected in a shift in the absorbance peak or the formation of a new peak, as NPs exhibit different plasmonic resonance based on their physical state. As NPs aggregate, their collective plasmonic fields interact, leading to these spectral changes. The more salicylic acid is present, the greater would be the extent of NP aggregation, leading to an increased absorbance ratio.

Further, the calibration curve was utilised to calculate the LOD for the sensing scheme, which was determined to be 0.55 ppm. This value is significantly lower than the general permissible limit for these adulterants, thereby asserting the sensitivity of the method. The recovery rate of the sensing scheme was found to be 96%, indicating high accuracy. Additionally, the method demonstrated a dynamic sensing range between 0.05 and 15 ppm with a sensitivity of 0.06 change in absorbance ratio/ppm. This broad dynamic range and high sensitivity make the scheme effective for detecting even trace amounts of salicylic acid in milk [83-85] (**Fig. 2.A.20**).

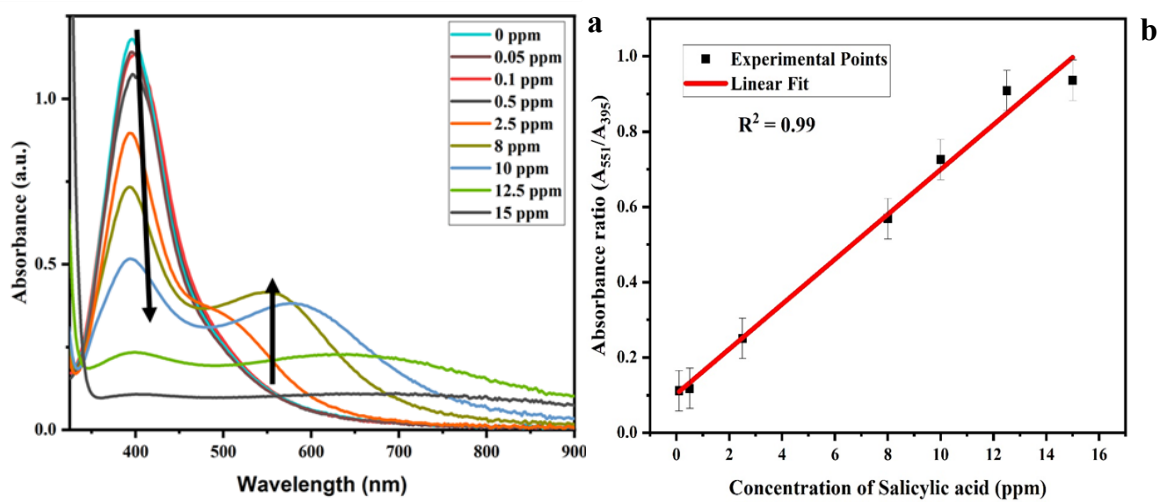

Figure 2.A.20.: (a) *UV-Vis plot of the synthesised WR-AgNPs in presence of salicylic acid in milk at varied concentrations, and* ***(b)*** *linear calibrated graph between absorbance ratio vs. concentration of salicylic acid in milk.*

2.A.5 Conclusion

In this study, a range of innovative and eco-friendly approaches for detecting milk adulterants were explored, focusing on the synthesis and application of plasmonic AgNPs. By employing various green and cost-effective methodologies, such as the use of green tea, cotton leaves, watermelon rind extract, and chemical routes with functionalizing agents such as L-cysteine, the synthesized AgNPs demonstrated exceptional stability, selectivity, and sensitivity across different detection platforms. These NPs displayed distinct optical properties, such as colorimetric responses and LSPR shifts, enabling efficient detection of toxic adulterants like melamine, hydrogen peroxide, formalin, and salicylic acid in milk.

The study highlights the versatility of AgNP-based colorimetric sensors. The interference-based method utilizing green tea extract provided a low LOD of 1.44 ppm for melamine, while the biosensing of hydrogen peroxide achieved an LOD of 8.46 ppm, underscoring the method's eco-friendliness and simplicity. Similarly, the watermelon rind-based synthesis demonstrated an LOD of 0.55 ppm for salicylic acid. Meanwhile, l-cysteine-functionalized AgNPs showed their utility in formalin detection, with an LOD of 3.51 ppm, further emphasizing the rapidity and user-friendliness of this approach.

These methodologies, characterized by their ease of implementation, minimal preprocessing requirements, and compatibility with simple spectroscopic techniques, stand out as practical alternatives to conventional detection methods. The integration of biological reducing agents not only enhanced the stability and functionality of the NPs but also aligned with sustainable practices, reducing environmental impact. Overall, this work underscores the potential of AgNPs as reliable, eco-friendly, and efficient sensors for ensuring the quality and safety of milk.

PART B: Colorimetric sensing of milk adulterants and contaminants with substrate*

Proliferation of adulteration and contamination in cattle milk is a century old global problem, which can only be curbed with proper detection measures. However, the currently available sensing architectures do not support simultaneous detection of multiple toxic adulterants and carcinogenic contaminants with high portability, and cost effectiveness. To address these lacunae, a paper based colorimetric sensor has been designed here that works on the principle of nanotechnology. The sensing system is sketched on a paper substrate that contains seven conduits attached with test regions for selective impregnation with respective functionalized AgNPs. The fabricated paper-based device can detect the presence of different milk adulterants and contaminants by displaying visible colorimetric response. This sensing approach is easy, portable, cost-effective, highly selective, sensitive, and has a lower LOD. This innovative technology requires no analytic or spectroscopic method to perform the detection—thereby making it an inexpensive point of care analysis platform for onsite detection of adulterants and contaminants in real samples.

The paper-based system could detect multiple toxic adulterants in milk e.g., melamine, hydrogen peroxide and formalin and other carcinogenic contaminants such as lead, cadmium, mercury and arsenic ions in milk simultaneously with high accuracy, sensitivity and selectivity. The proposed sensing unit is based on the synergy of paper-based sensing and nanotechnology.

2.B.1 Synthesis, functionalisation of AgNPs and pretreatment of milk

2.B.1.1 Synthesis of maleic acid functionalised AgNPs

Preparation of reducing and functionalising agents: 1 mM $AgNO_3$ solution was prepared by adding 0.0169 g in 100 mL of DW. Following which, 2mM of $NaBH_4$ solution was prepared by adding 0.008 g in 100 mL of DW for a duration of 5 min at room temperature

*This section of the thesis is published (early publication) as a patent (U. Das *et al.*, Patent application no.: 202331046391)

at a stirring rate of 600 rpm. To properly cap and encapsulate the NPs 1% TSC solution was prepared for which 1 g of TSC was dissolved in 100 mL of DW. For functionalisation of AgNPs, 18 Mm maleic acid solution was prepared for which 0.042 g of maleic acid was added to 20 mL of DW solution and stirred at room temperature for a duration of 10 min at a rate of 600 rpm [86].

Preparation of functionalised NPs: To prepare the NPs, 28 mL of $NaBH_4$ was continuously stirred at 800 rpm. To it, 14 mL of 1 mM $AgNO_3$ solution was added dropwise. The colour of the solution changed to yellow colour from colourless. To prevent aggregation of particles 2 mL of TSC was added to this colloidal solution under continuous stirring at 800 rpm at room temperature. The stirring of NPs was continued for 20 min for uniform encapsulation and capping of each NP. Following this 2 mL of 18 mM maleic acid solution was added to the synthesised NP solution which was then stirred at 900 rpm for 30 min at room temperature for uniform surface functionalisation of the citrate capped NPs with the polyphenolic group of maleic acid. The pH of the solution was then adjusted to 7 by addition of 0.1 M NaOH solution under continuous stirring at 900 rpm. The resulting solution was deep yellow in colour indicating formation of smaller sized maleic acid functionalised AgNPs [86].

2.B.1.2 Synthesis of l-cysteine functionalised AgNPs

AgNPs were prepared as per the same protocol reported in the previous study (section 2.A.3.1).

2.B.1.3 Synthesis of *Camellia sinensis* encapsulated AgNPs

Synthesis of reducing and capping agent: 1 mM $AgNO_3$ solution was prepared by following the same protocol as reported in section (2.B.1.1). Following which, green tea extract was prepared for which pre-processed green tea was used. 3 g of dried green tea leaves were weighed and then washed with DW. It was then added to 50 mL of DW, this mixture was then heated at 60^{o}C for a duration of 15 min. After which the extract was filtered twice by using a Whatman no. 1 filter paper [87].

Preparation of the encapsulated NPs: 40 mL of 1 mM $AgNO_3$ solution was stirred continuously at a rate of 600 rpm. To this solution 800 µL of green tea extract was added and the resulting solution was stirred at a 600 rpm in room temperature conditions. To this solution 200 µL of 0.1 M NaOH was added which acted as a catalyst and immediately changed the colour of the solution to orangey yellow [87].

2.B.1.4 Synthesis of PVA functionalised BRB reduced AgNPs

Synthesis of reducing and functionalising agent: Precursor $AgNO_3$ was prepared by following the same protocol as reported in the previous section (section 2.B.1.1). Following which, the BRB was prepared, for which 50 g of root bulb was chopped into small pieces, washed properly and dried in an oven at 100ºC for 12 h. To this dried BRB, 200 mL of DW was added and the resulting mixture was heated at 100ºC for 1 ½ h. Then this extract was filtered twice by using Whatman filter paper no. 1. For functionalisation of NPs, 3% PVA solution was prepared for which 3 g of PVA was dissolved in 100 mL of DW by stirring it at 60ºC for a duration of 3 h at a rate of 900 rpm [88,89].

Preparation of functionalised AgNPs: 40 mL of 10 mM $AgNO_3$ solution was taken in a 50 ml beaker and was stirred continuously, to it 3.2 mL of BRB extract was added and the solution was stirred at 900 rpm at 120ºC for a duration of 30 min. Following this, the 5 mL of 3% PVA solution was added dropwise and the resulting solution was stirred at 800 rpm for 1 h at 60º C. The pH of the solution was then adjusted to 7 by addition of 0.1 M NaOH solution under continuous stirring at 900 rpm. The resulting solution was brown in colour indicating formation of PVA functionalised AgNPs [88,89].

2.B.1.5 Synthesis of citric acid functionalised AgNPs

Synthesis of reducing and functionalising agent: Precursor salt $AgNO_3$, the reducing agent, and the capping agent were prepared by following the same protocol as reported in section 2.B.1.1. For functionalisation of NPs, 6.4 mM citric acid solution was prepared for which 0.024 g of citric acid was added to 20 mL of DW and stirred for a duration of 5 min at a rate of 600 rpm at room temperature [90].

Preparation of functionalised NPs: AgNPs were prepared as per the same protocol reported in the previous study (section 2.B.1.1). Following which, the NPs were functionalised for which 3 mL of 6.4 mM citric acid solution was added to the synthesised NP solution. It was then stirred at 900 rpm for 15 min at room temperature for uniform surface functionalisation of the AgNPs with citric acid. The pH of the solution was then adjusted to 7 by addition of 0.1 M NaOH. The resulting solution was yellow in colour indicating formation of citric acid functionalised AgNPs [90].

2.B.1.6 Synthesis of salicylic acid functionalized AgNPs

Preparation of reducing and functionalising agent: Precursor salt $AgNO_3$, the reducing agent, and the capping agent were prepared by following the same protocol as reported in the previous section (section 2.B.1.1). For functionalisation of NPs, 13.03 mM salicylic acid solution was prepared for which 0.036 g of salicylic acid was added to 20 mL of DW and stirred at 90^{o}C for a duration of 45 min at a rate of 900 rpm [91].

Preparation of functionalised NPs: AgNPs were prepared as per the same protocol reported in the previous study (section 2.B.1.1). Following this, 2 mL of 13.03 mM salicylic acid solution was added to the synthesised NP solution which was then stirred at 900 rpm for 20 min at room temperature for uniform surface functionalisation of the citrate capped NPs with salicylic acid. The pH of the solution was then adjusted to 7 by addition of 0.1 M NaOH solution. The resulting solution was yellow in colour indicating formation of salicylic acid functionalised AgNPs [91].

2.B.1.7 Synthesis of l-glutamine functionalised AgNPs

Preparation of reducing and functionalising agent: Precursor salt $AgNO_3$, the reducing agent, and the capping agent were prepared by following the same protocol as reported in the previous section (section 2.B.1.1). For functionalisation of NPs, 14.3 mM l-glutamine solution was prepared for which 0.042 g of l-glutamine was added to 20 mL of DW and stirred at 60^{o}C for a duration of 30 min at a rate of 1000 rpm [92].

Preparation of functionalised NPs: AgNPs were prepared as per the same protocol reported in the previous study (section 2.B.1.1). Following this, 1.5 mL of 14.3 mM l-

glutamine solution was added to the synthesised NP solution which was then stirred at 900 rpm for 30 min at room temperature for uniform surface functionalisation of the citrate capped AgNPs with l-glutamine. The pH of the solution was then adjusted to 7 by addition of 0.1 M NaOH solution under continuous stirring at 900 rpm. The resulting solution was greenish yellow in colour indicating formation of l-glutamine functionalised AgNPs [92].

2.B.1.8. Pretreatment of milk

For detection, milk needs to be pretreated to remove the interfering fats and proteins as they may cause hindrance in the detection process. Accordingly, 200 mL of milk was initially pre-treated with 10 mL of vinegar, to obtain the whey. The mixture was then stirred properly with a glass rod and then vortexed for 5 min. The pH of the mixture was adjusted to 7 by addition of 3M NaOH. This whey or milk supernatant was then filtered twice using a Whatman filter paper no. 1. This milk supernatant was spiked with various concentrations of different adulterants and heavy metal ions as contaminants such as melamine (0.001-100 ppm), formalin (0.37-370000 ppm), hydrogen peroxide (0.003-300000 ppm), mercury ion (Hg^{2+}) (0.0001-100 ppm), arsenic ion (As^{3+}) (0.001-100 ppm), cadmium ion (Cd^{2+}) (0.001-100 ppm) and lead ion (Pb^{2+}) (0.001-1000 ppm).

2.B.2. Characterisation of functionalised AgNPs

2.B.2.1 Characterisation of maleic acid functionalised AgNPs

To ensure the formation and determine the characteristics of the synthesized AgNPs, they were first subjected to UV−Vis spectroscopic analysis. This confirmation of formation of AgNPs was based on the observation of a distinct absorbance spectrum at approximately 407 nm [42]. Furthermore, XRD diffractogram confirmed the structural orientation of the NPs to be FCC and crystalline, with diffraction peaks at (111), (200), (220), and (311) [43]. TEM study confirmed that the synthesized AgNPs exhibited a spherical shape with a mean diameter of 3.90 nm and were of size ranging between 1 and 10 nm [44] (**Fig. 2.B.1**).

2.B.2.2 Characterisation of l-cysteine functionalised AgNPs

Similarly, all the characterisations of the l-cysteine functionalised AgNPs are already reported in section (section 2.A.3.2).

2.B.2.3 Characterisation of green tea encapsulated AgNPs

All the characterisations were performed as per reported in section 2.B.2.1. A distinct absorbance peak was obtained at 405 nm [42]. XRD study revealed that the synthesised NPs are FCC and crystalline in nature [43]. TEM data confirmed that the synthesized NPs exhibited a spherical shape with a mean diameter of 8.31 nm and size ranging between 2 and 22 nm [44] (**Fig. 2.B.2**).

2.B.2.4 Characterisation of PVA functionalised BRB reduced AgNPs

All the characterisations were performed as per reported in section 2.B.2.1. Distinct absorbance peak was obtained at 406 nm [42]. Furthermore, XRD study revealed that the synthesised NPs were FCC crystalline structure [43]. TEM data confirmed that the synthesized NPs exhibited a spherical shape with a mean diameter of 11.86 nm and size ranging between 4 and 22 nm [44] **(Fig. 2.B.3**).

2.B.2.5 Characterisation of citric acid functionalised AgNPs

All the characterisations were performed as per reported in the previous section 2.B.2.1. Distinct absorbance peak was obtained at 390 nm [42]. Furthermore, XRD study revealed that the synthesised NPs were FCC crystalline in structure [43]. TEM data confirmed that the synthesized NPs exhibited a spherical shape with a mean diameter of 22.35 nm and size ranging between 5 and 45 nm [44] (**Fig. 2.B.4**).

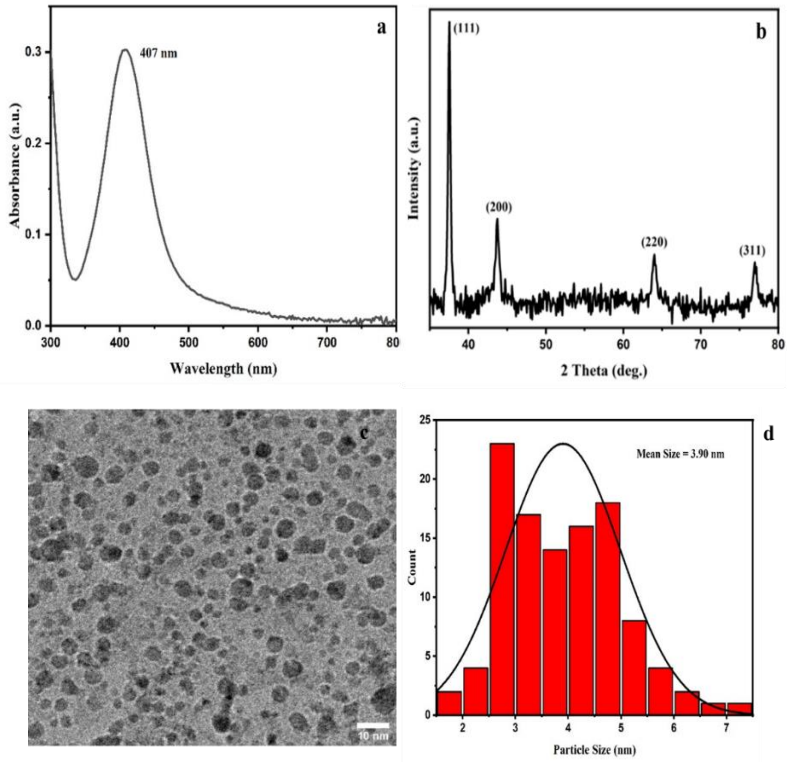

Figure 2.B.1: *Characterisation of MA-AgNPs* ***(a)*** *UV-Vis spectrum,* ***(b)*** *XRD pattern,* ***(c)*** *TEM image, and* ***(d)*** *size distribution analysis from TEM.*

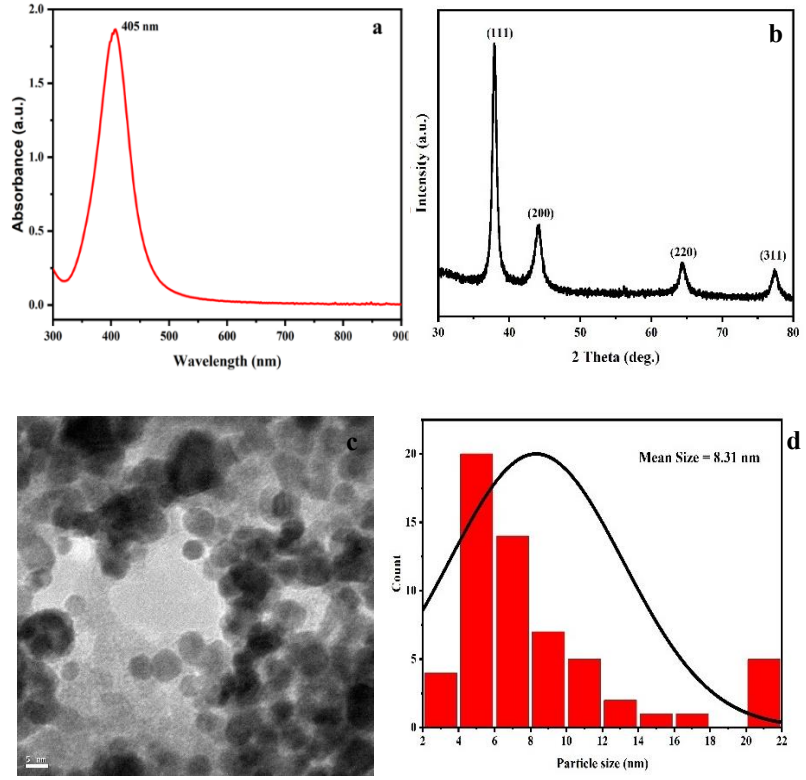

Figure 2.B.2: *Characterisation of GT reduced AgNPs* ***(a)*** *UV-Vis spectrum,* ***(b)*** *XRD pattern,* ***(c)*** *TEM image, and* ***(d)*** *size distribution analysis from TEM.*

2.B.2.6 Characterisation of salicylic acid functionalised AgNPs

All the characterisations were performed as per reported in the previous section. Distinct absorbance peak was obtained at 392 nm [42]. Furthermore, XRD study, suggested that the synthesised NPs were FCC crystalline in nature [43]. TEM data confirmed that the synthesized NPs exhibited a spherical shape with a mean diameter of 8.64 nm and size ranging between 1 and 16 nm [44] (**Fig. 2.B.5**).

2.B.2.7 Characterisation of l-glutamine functionalised AgNPs

All the characterisations were performed as per reported in the previous section. Distinct absorbance peak was obtained at 394 nm [42]. Furthermore, XRD study confirmed that the synthesised NPs possess an FCC crystalline structure [43]. TEM data confirmed that the synthesized NPs exhibited a spherical shape with a mean diameter of 21.13 nm and size ranging between 5 and 55 nm [44] (**Fig. 2.B.6**).

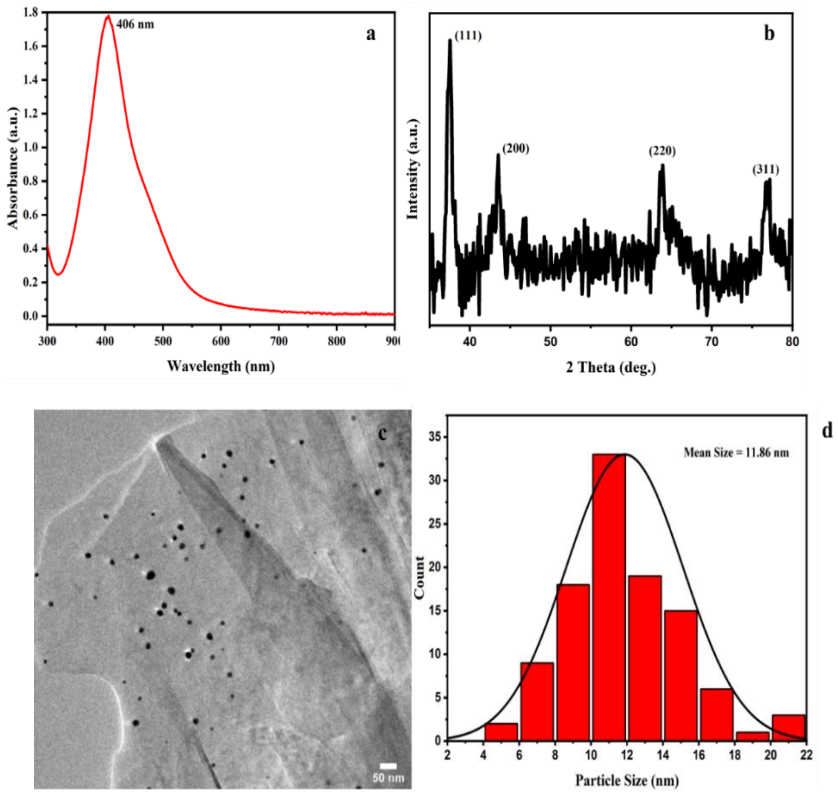

Figure 2.B.3.: *Characterisation of PVA-AgNPs* ***(a)*** *UV-Vis spectrum,* ***(b)*** *XRD pattern,* ***(c)*** *TEM image, and* ***(d)*** *size distribution analysis from TEM.*

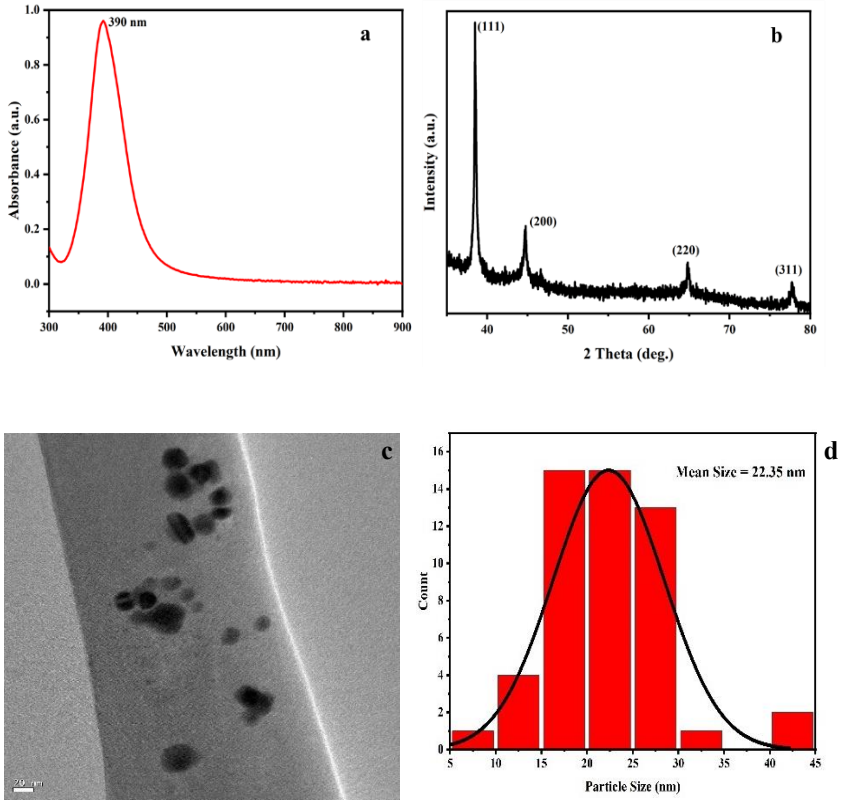

Figure 2.B.4: *Characterisation of CA-AgNPs* ***(a)*** *UV-Vis spectrum,* ***(b)*** *XRD pattern,* ***(c)*** *TEM image, and* ***(d)*** *size distribution analysis from TEM.*

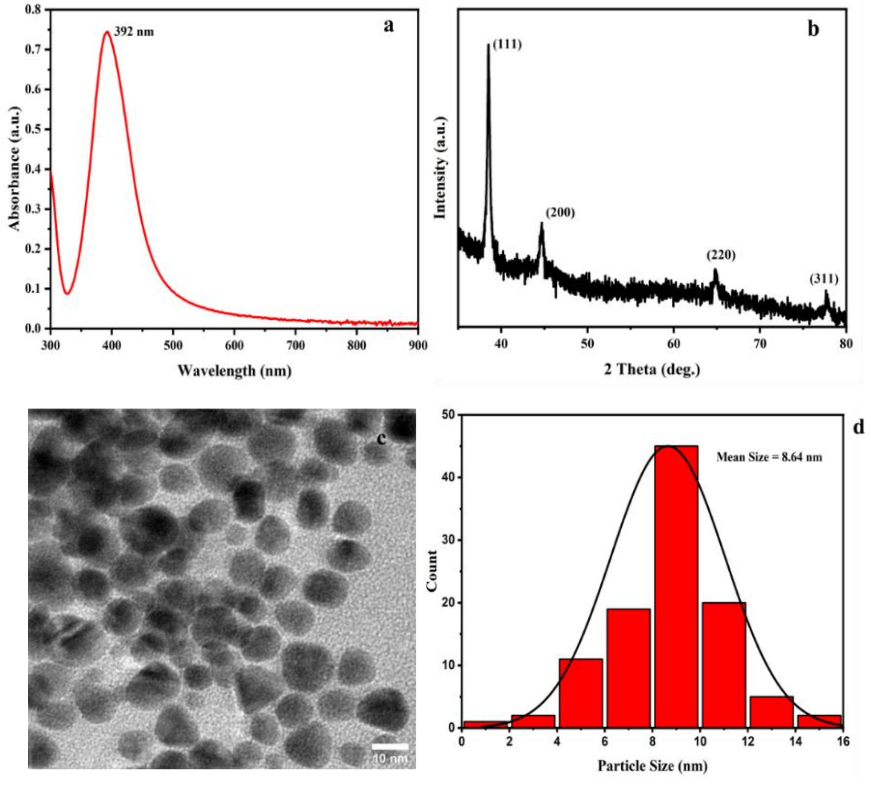

Figure 2.B.5: *Characterisation of SA-AgNPs* ***(a)*** *UV-Vis spectrum,* ***(b)*** *XRD pattern,* ***(c)*** *TEM image, and* ***(d)*** *size distribution analysis from TEM.*

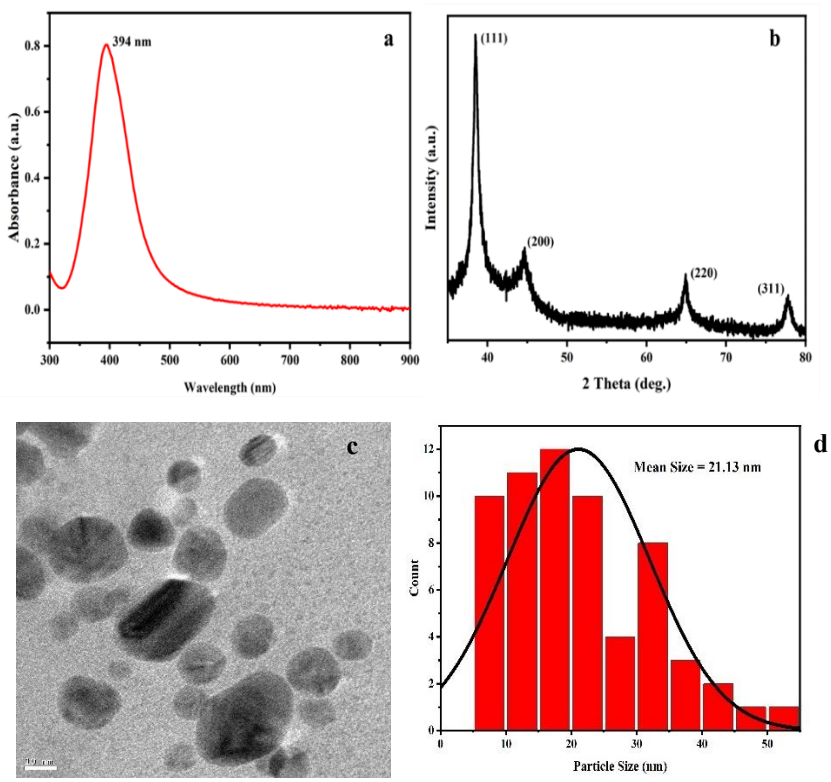

Figure 2.B.6: *Characterisation of l-glutamine-AgNPs* ***(a)*** *UV-Vis spectrum,* ***(b)*** *XRD pattern,* ***(c)*** *TEM image, and* ***(d)*** *Size distribution analysis from TEM.*

2.B.3 Fabrication of paper-based platform

At first, a geometrical pattern in the form of diverging conduits having common centre was fabricated on a photopaper with the help of a laser printer. Then a hydrophobic barrier was stamped with the help of paraffin wax which was used as hydrophobic ink using a stamp of similar dimension as that of the design printed on the photopaper. The paper substrate was then heated in an oven at 100°C to allow the hydrophobic ink to permeate into the photopaper outside the boundary region of the multi-finger conduits. Then, Whatman no. 1 filter paper of diameter 1 cm was attached to each leg end. It was then treated with 200 µL of different selectively functionalized NPs and was allowed to get air dried for 1 h at room temperature. Subsequently, each leg was then further treated with the selectively functionalised NPs and allowed to dry.

To ensure uniform flow of the milk supernatant through each channel, a 3D-modeled substrate was fabricated to support the detection scheme. This 3D-printed setup consists of three parts.

Bottom Layer: This layer is cylindrical in shape with a height of 15 mm, outer diameter of 80 mm and an inner diameter of 75 mm. It was made up of tough polylactic acid (PLA) which was used to hold the paper substrate.

Middle Layer: This layer having similar composition with bottom layer facilitates uniform liquid flow through preferably seven channels separated by hydrophobic barriers. It contains seven conduits, each of width 10 mm and a length of 30 mm, and a central opening with a diameter of 30 mm. The middle layer has a height of 5 mm and a diameter of 74.5 mm, fitting perfectly on the base plate with the wax-coated paper sandwiched between the two substrates. The diameter of this layer was precisely maintained to ensure it fits perfectly onto the bottom layer when pressed together.

Top Layer: This layer also has a similar composition with bottom and middle layer aids in visualizing the colour change in NPs. It has a height of 4 mm and a diameter of 74.5 mm, with one central opening/hole of 30 mm diameter and seven openings/holes at the ends of the conduits, each 10 mm in diameter. This layer was simply attached to the middle layer using an adhesive.

The liquid, when poured at the centre of the substrate, flows through the channels, and collects at the ends of the conduits, where the functionalized AgNPs are located (**Fig. 2.B.7**).

Figure 2.B.7: *The paper based microfluidic device.*

2.B.4 Colorimetric sensing in paper-based platform

Functionalization refers to surface modification of the AgNPs with suitable bioactive molecules. These molecules interact with a specific analyte either via hydrogen bonding or electron donor interaction, resulting in aggregation/oxidation of NPs, which is responsible for the visible colour change.

5 ml of milk supernatant spiked with various adulterants and contaminants were poured at the centre of the substrate, milk flows through the channels and finally reaches the leg end where it interacts with the functionalised AgNPs impregnated on the paper substrate.

2.B.4.1 Melamine sensing

For the detection of melamine, AgNPs were surface-functionalized with maleic acid, which contains two carboxylic groups. This colorimetric change can be observed in paper-based substrates when melamine-adulterated milk comes into contact with the maleic acid-functionalized AgNPs. The colour of the paper substrate changed from light yellow to brown or purple with increasing concentrations of melamine (0.001-100 ppm) in milk. The colorimetric response time of this method ranges from 5 to 15 min. At higher analyte concentrations, the colour change occurs more rapidly, and the response time decreases accordingly (**Fig. 2.B.8**).

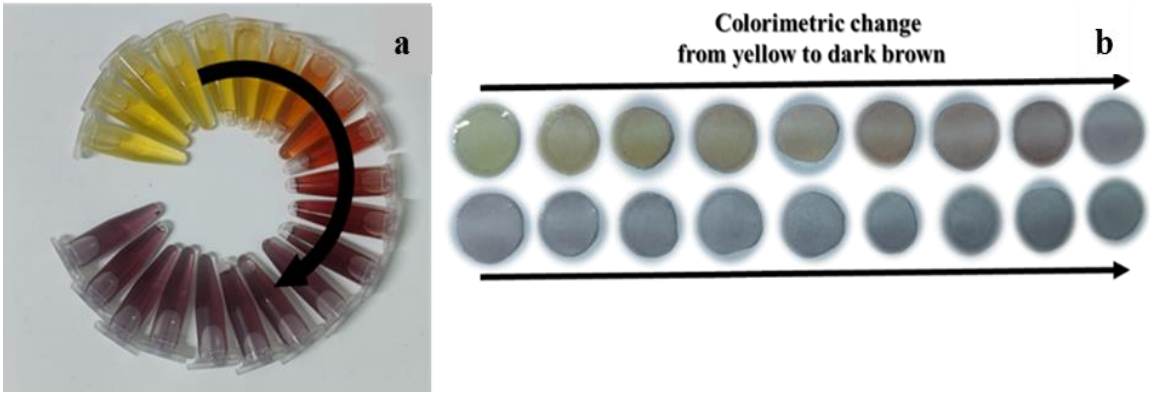

Figure 2.B.8: ***(a)*** *Liquid based sensing, and* ***(b)*** *sensing in paper-based platform of melamine in milk.*

2.B.4.1.1 Mechanism

Carboxylic groups in maleic acid interact with the NH_2 groups of melamine, through hydrogen bonding. This interaction decreases the interparticle distance between the AgNPs, causing a colorimetric change. The colour of the NPs solution changes from bright yellow to orange, red, brown, and finally purple as the interparticle distance decreases [17].

2.B.4.1.2 Sensor performance metrics

For determination of LOD for melamine, the change in colour intensity of AgNPs in the presence of melamine on the paper device was recorded. In order to quantify the colorimetric data, smartphone camera (Model XIAOMI POCO F5, Aperture F1.8) was used to capture and record the images of the paper substrate in .jpeg format. The photographs were then subsequently processed using Image J software by selecting a circular area as region of interest for each functionalized paper substrate to extract the mean RGB (red, green and blue) values. RGB additive model is a non-uniform colour space, hence each component was normalized where r (equation **2.B.1**), g (equation **2.B.2**), and b (equation **2.B.3**), values were calculated as follows:

$$r = \frac{R}{R+G+B} \quad \textbf{(2.B.1)}$$

$$g = \frac{G}{R+G+B} \quad \textbf{(2.B.2)}$$

$$b = \frac{B}{R+G+B} \quad \textbf{(2.B.3)}$$

In this case, a calibration graph was plotted with the ratio [B/(R+G+B)] against the concentration of melamine, as it resulted in a linear relationship. This graph facilitated the determination of the LOD using the specified formula. The LOD for the paper-based sensing scheme was determined to be 0.76 ppm [93-95] (**Fig. 2.B.9**).

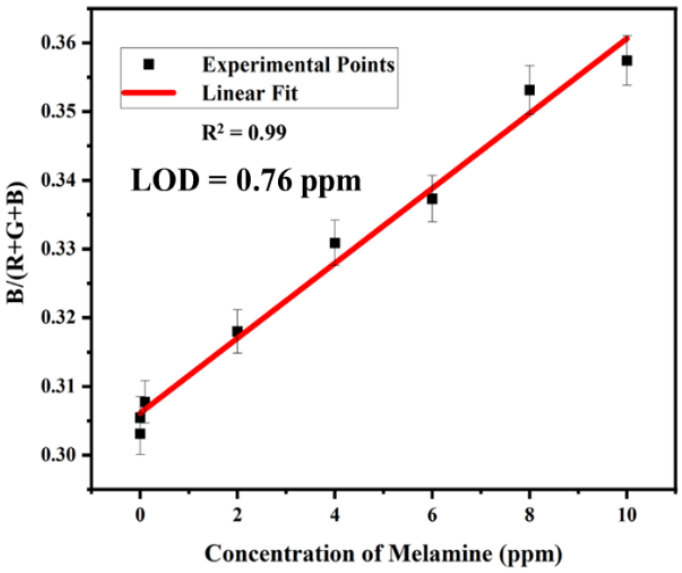

Figure 2.B.9: *Calibration curve for melamine adulterated milk.*

2.B.4.2 Formalin sensing

For detecting formalin, AgNPs were surface-functionalized with l-cysteine. The colour of the paper substrate changed from greenish-yellow to brown with increasing concentrations of formalin (0.37-370000 ppm) in milk. The colorimetric response time of this method ranges from 2 to 5 min (**Fig. 2.B.10**).

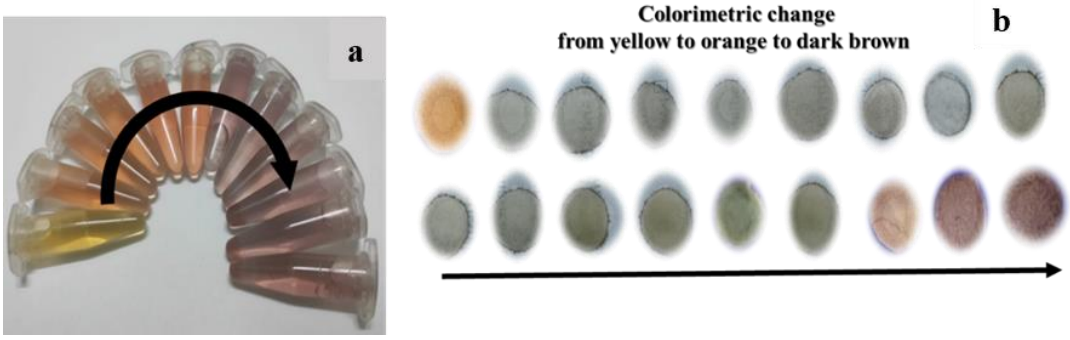

Figure 2.B.10: ***(a)*** *Liquid based sensing, and* ***(b)*** *sensing in paper-based platform of formalin in milk.*

2.B.4.2.1 Mechanism

The amino (-NH_2) groups in l-cysteine reacted with the aldehyde (-CHO) group in formaldehyde, leading to the formation of Schiff bases. This chemical interaction alters the surface properties of the NPs, inducing aggregation and thereby reducing the

interparticle distance. The resulting aggregation caused a visible colour change due to a shift LSPR band in AgNPs. Additionally, the porous nature of the filter paper facilitates the smooth movement of NPs, further enhancing their aggregation and reducing interparticle distance [73,75,76].

2.B.4.2.2 Sensor performance metrics

The LOD was estimated using RGB values which were obtained from the previous method stated above. A calibration graph was plotted with the ratio [R/(R+G+B)] against the concentration of formalin, as it resulted in a linear relationship. This graph facilitated the determination of the LOD using the specified formula. The LOD for the paper-based sensing scheme was determined to be 4.53 ppm [93-95] (**Fig. 2.B.11**).

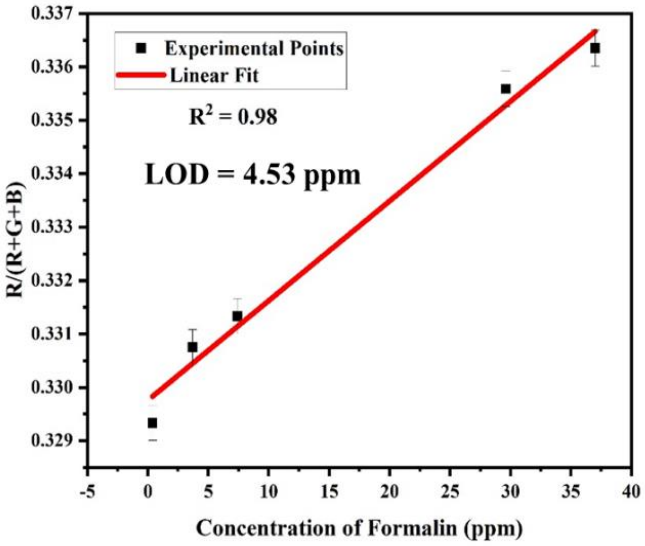

Figure 2.B.11: *Calibration curve for formalin adulterated milk.*

2.B.4.3 Hydrogen peroxide sensing

For detecting hydrogen peroxide, AgNPs are capped with the polyphenolic groups of green tea. The colour of the paper substrate changed from orange yellow to light yellow/colourless with increasing concentrations of hydrogen peroxide (0.003-300000 ppm) in milk. The colorimetric response time of this method ranges from 1 to 15 min (**Fig. 2.B.12**).

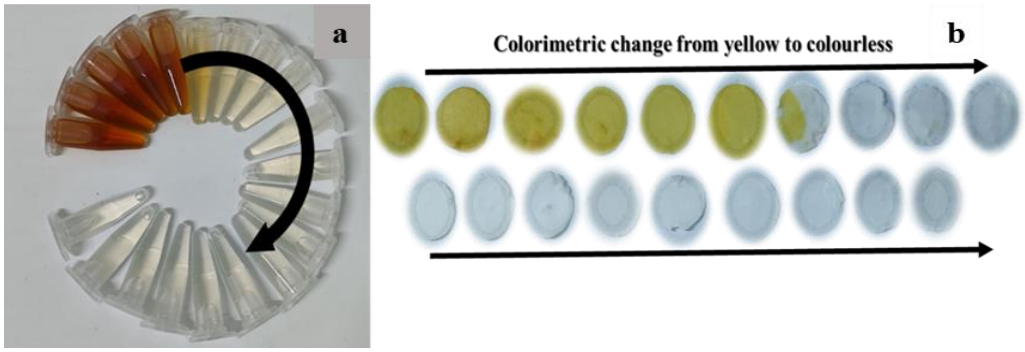

Figure 2.B.12: (a) *Liquid based sensing, and* ***(b)*** *sensing in paper-based platform of hydrogen peroxide in milk.*

2.B.4.3.1 Mechanism

The hydrogen peroxide molecules can easily oxidize the silver atoms on the surface of the NPs as the NPs are not stabilised or capped. In this redox reaction, hydrogen peroxide accepts electrons from the silver atoms, which leads to the formation of Ag^{+} and hydroxide ions (OH^{-}). The silver atoms (Ag^{0}) lose electrons to become Ag^{+}. These ions are then released from the surface of the AgNPs into the surrounding solution. The oxidation of surface silver atoms results in a reduction in the size of the NPs and can lead to changes in their shape and surface structure, which is responsible for the colorimetric change in NPs in presence of hydrogen peroxide [96].

2.B.4.3.2 Sensor performance metrics

The LOD was estimated using RGB values which were obtained from the previous method stated above. A calibration graph was plotted with the ratio [B/(R+G+B)] against the concentration of hydrogen peroxide, as it resulted in a linear relationship. This graph facilitated the determination of the LOD using the specified formula. The LOD for the paper-based sensing scheme was determined to be 5.6 ppm [93-95] (**Fig. 2.B.13**).

2.B.4.4 Mercury sensing

For detecting mercury, AgNPs were surface-functionalized with PVA and reduced with BRB extract. The colour of the paper substrate changed from brown to colourless with increasing concentrations of mercury (0.0001-100 ppm) in milk. The colorimetric response time of this method ranges from 1 to 20 min (**Fig. 2.B.14**).

2.B.4.4.1 Mechanism

AgNPs were coated with PVA, which is a polymer that stabilizes the AgNPs and prevents their aggregation. PVA has numerous hydroxyl groups (-OH) that can interact with metal ions, including Hg^{2+} ions. When Hg^{2+} ions are introduced into the solution containing PVA-capped AgNPs, they can interact with the silver atoms of the NPs. This interaction often involves the reduction of Hg^{2+} to elemental mercury (Hg^0), which results in immediate oxidative dissolution of AgNPs. This process involves the oxidation of all the Ag^0 in a NPs to Ag^+ in the presence of Hg^{2+}. When AgNPs were dissolved and converted into Ag^+, they lose their LSPR properties, resulting in a loss of the yellow colour. This causes the solution to turn colourless as the NPs get oxidized and dissolved [97].

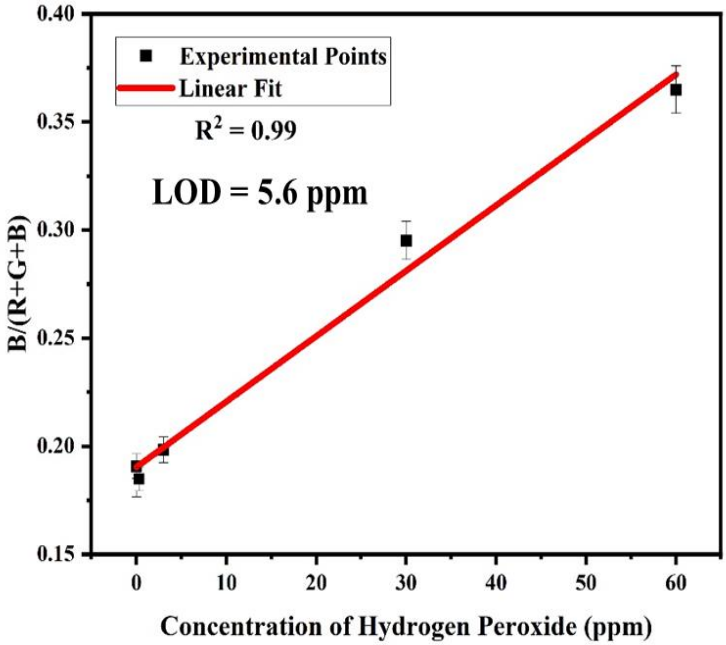

Figure 2.B.13: *Calibration curve for hydrogen peroxide adulterated milk.*

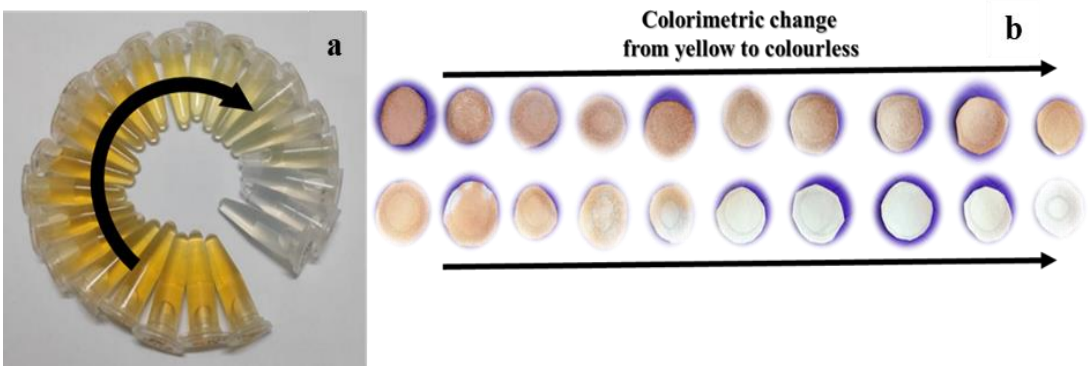

Figure 2.B.14: (a) *Liquid based sensing, and* ***(b)*** *sensing in paper-based platform mercury in milk.*

2.B.4.4.2 Sensor performance metrics

The LOD value in this case was determined using the HSV model. For accurate LOD calculation, a linearly calibrated graph was required, which cannot be reliably obtained using the RGB model due to its nonlinear nature in representing colour intensities. The HSV model, described by a cylindrical geometry with three parameters—hue, saturation, and value—was chosen to quantify the colorimetric data. RGB values extracted from the images were converted to the HSV model using standard algorithms, enabling a more accurate representation of colorimetric changes and LOD determination. The algorithms were as follows (**equation 2.B.4; 2.4.5; 2.B.6; 2.B.7** & **2.B.8**) [98-101]:

$$V = \max(R, G, B) \quad \textbf{(2.B.4)}$$

$$S = \begin{cases} 0 & \text{if } V = 0 \\ \dfrac{V - \min(R,G,B)}{V} & \text{if } V > 0 \end{cases} \quad \textbf{(2.B.5)}$$

$$\Delta = \max - \min \quad \textbf{(2.B.6)}$$

$$H = \begin{cases} 0 & \text{if } S = 0 \\ 60^o \text{ x } (\frac{G-B}{\Delta}) & \text{if max} = R \\ 60^o \text{ x } (\frac{B-R}{\Delta} + 2) & \text{if max} = G \\ 60^o \text{ x } (\frac{R-G}{\Delta} + 4) & \text{if max} = B \end{cases} \quad \textbf{(2.B.7)}$$

$$H = H + 360^o \quad \text{if } H < 0 \quad \textbf{(2.B.8)}$$

Incorporating the mentioned algorithms, a custom Python code was developed with necessary libraries ‘panda’ and ‘colorsys’ to transform the obtained mean RGB values to HSV values.

A calibration graph was plotted with the value against the concentration of mercury, resulting in a linear relationship. This graph facilitated the determination of the LOD using the specified formula. The LOD for the paper-based sensing scheme was determined to be 0.87 ppm [98-101] (**Fig. 2.B.15**).

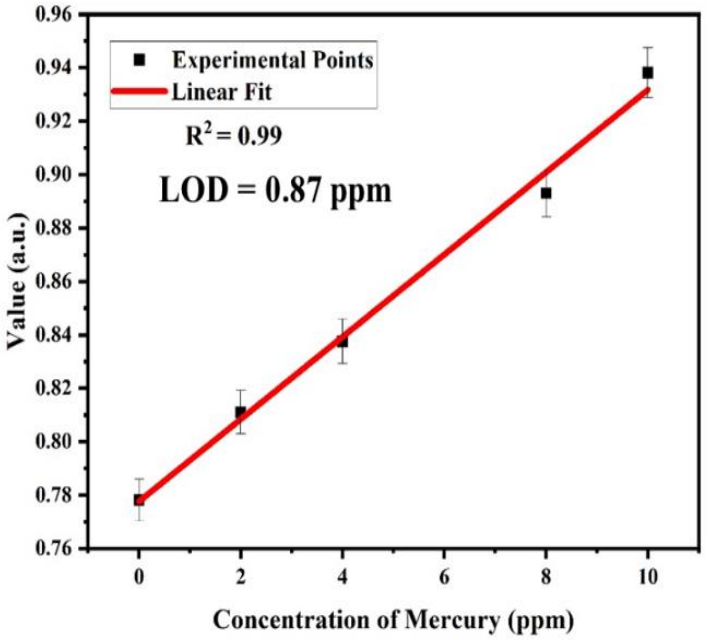

Figure 2.B.15: *Calibration curve for mercury adulterated milk.*

2.B.4.5 Arsenic sensing

For the detection of arsenic, AgNPs are surface-functionalized with citric acid. The colour of the paper substrate changed from light yellow to brown or purple with increasing concentrations of arsenic (0.001-100 ppm) in milk. The colorimetric response time of this method ranges from 1 to 5 min (**Fig. 2.B.16**).

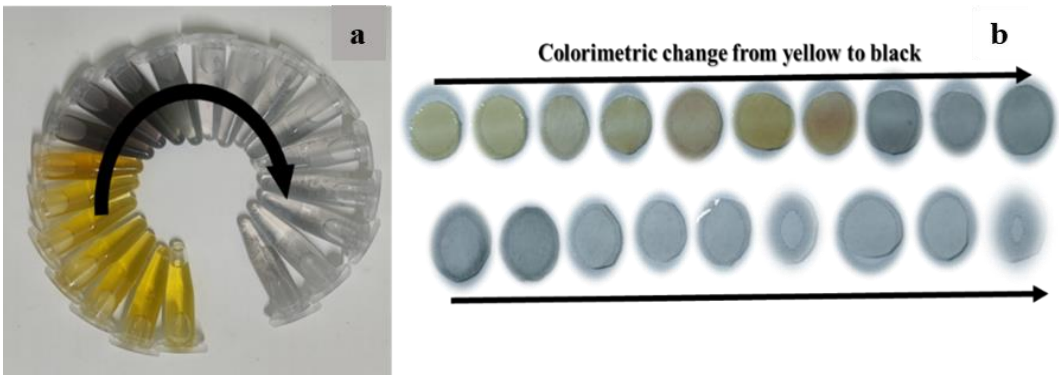

Figure 2.B.16: (a) *Liquid based sensing, and* ***(b)*** *sensing in paper-based platform sensing in paper-based platform arsenic in milk.*

2.B.4.5.1 Mechanism

Citric acid contains three carboxyl groups (-COOH) and one hydroxyl group (-OH) that can interact with metal ions. When arsenic ions are introduced into the solution containing citric acid-functionalized AgNPs, they can interact with the functional groups on the citric acid. This interaction can involve complexation, where the As^{3+} bind to the carboxyl groups of citric acid. The binding of As^{3+} to the citric acid molecules on the surface of the AgNPs can lead to coordination. This coordination acts as a "crosslink," causing aggregation of the AgNPs. When the NPs aggregate, the LSPR band shifts, leading to a visible colour change. Typically, the colour change can range from yellow to brown or red, depending on the degree of aggregation and the concentration of the ions [102].

2.B.4.5.2 Sensor performance metrics

The LOD was estimated using HSV values which were obtained from the previous method stated above (section 2.B.4.4.2). A calibration graph was plotted with the hue against the concentration of arsenic, as it resulted in a linear relationship. As a linear calibration plot is crucial for estimation of LOD. This graph facilitated the determination of the LOD using the specified formula, which was found to be 0.65 ppm [98-101] (**Fig. 2.B.17**).

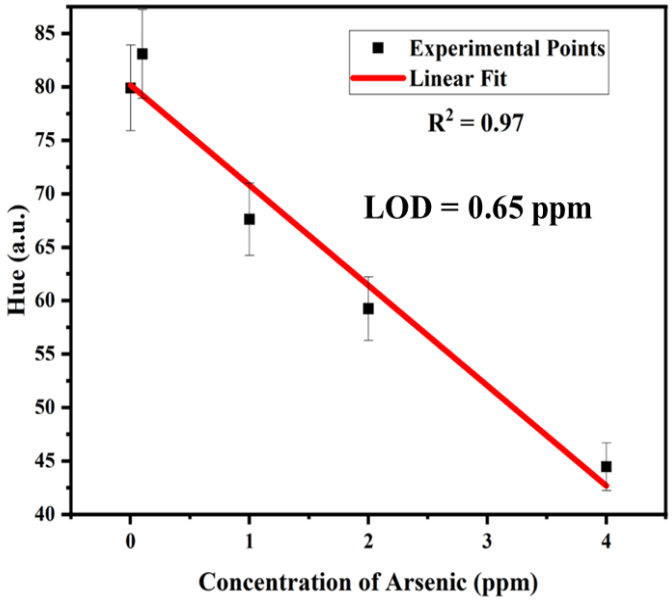

Figure 2.B.17: *Calibration curve for arsenic adulterated milk.*

2.B.4.6 Cadmium sensing

For the detection of cadmium, AgNPs were surface-functionalized with salicylic acid. Typically, the colour change can be observed from yellow to brown or red, depending on the extent of aggregation and the concentration of cadmium ions (0.001-100 ppm) in milk. The colorimetric response time of this method ranges from 1 to 5 min (**Fig. 2.B.18**).

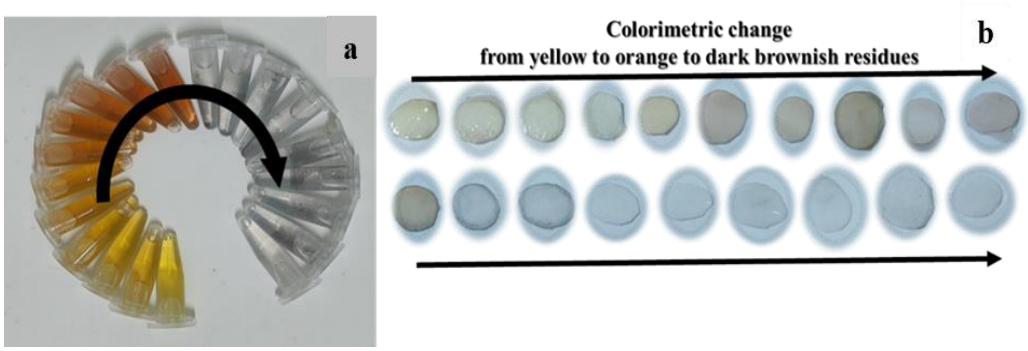

Figure 2.B.18: ***(a)*** *Liquid based sensing, and* ***(b)*** *sensing in paper-based platform cadmium in milk.*

2.B.4.6.1 Mechanism

Salicylic acid possesses both a carboxyl group (-COOH) and an ortho-phenolic hydroxyl group (-OH), which together provide a bidentate chelating site. When milk spiked with Cd^{2+} were introduced into a solution containing salicylic acid–functionalized AgNPs, they preferentially coordinate with the oxygen donor atoms of these two groups. This chelation stabilizes the Cd^{2+}–ligand complex and enables the ion to act as a bridge between salicylic acid molecules on different NPs. As a result, aggregation of the AgNPs occur. The aggregation perturbs the NPs' LSPR peak, leading to a red-shift or peak broadening which results in a visible color change in the solution [103].

2.B.4.6.2 Sensor performance metrics

The LOD was estimated using RGB values which were obtained from the previous method stated in section 2.B.4.1.2. A calibration graph was plotted with the red intensity against the concentration of cadmium ion, as it resulted in a linear relationship. As a linear calibrated graph is necessary for estimation of LOD. This graph facilitated the

determination of the LOD using the specified formula, which was found to be 0.73 ppm [93-95] (**Fig. 2.B.19**).

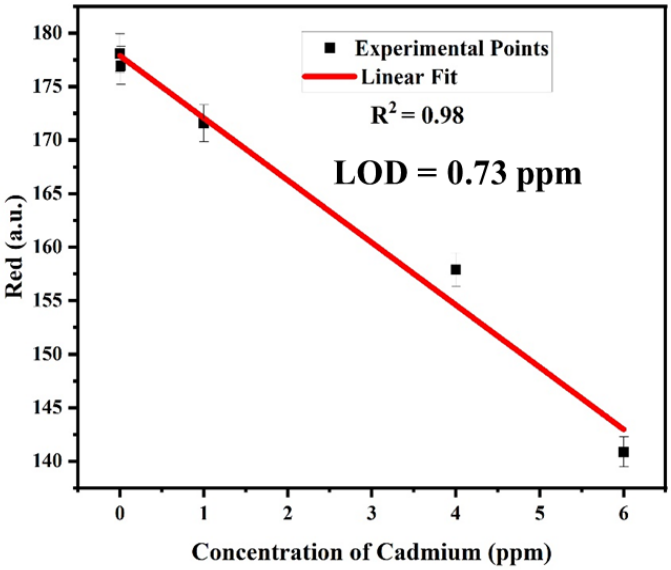

Figure 2.B.19: *Calibration curve for cadmium adulterated milk.*

2.B.4.7. Lead sensing

For the detection of lead ion, AgNPs were surface-functionalized with l-glutamine. The colour of the paper substrate changed from light yellow to brown with increasing concentrations of lead (0.001-1000 ppm) in milk. The colorimetric response time of this method ranges from 5 to 20 min. The colour change occurs more rapidly with higher lead concentrations, and the response time shortens accordingly with increasing analyte amounts (**Fig. 2.B.20**).

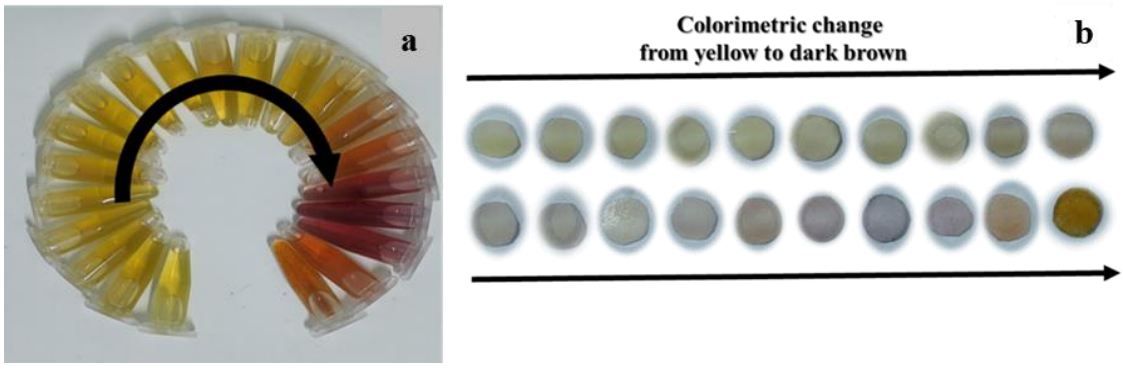

Figure 2.B.20: ***(a)*** *Liquid based sensing, and* ***(b)*** *sensing in paper-based platform lead in milk.*

2.B.4.7.1 Mechanism

L-glutamine is a naturally occurring amino acid, having two amine group (-NH_2) and one carboxyl groups (-COOH) in its molecular structure. These functional groups can interact with lead ions through coordination chemistry. When lead ions (Pb^{2+}) are present in the solution containing l-glutamine-functionalized AgNPs, they can form coordination complexes with the functional groups on l-glutamine. Lead ions have a high affinity for nitrogen and oxygen donor atoms, which are present in the amine and carboxyl groups of l-glutamine. The binding of lead ions to the functional groups on l-glutamine induces aggregation of the AgNPs. The aggregation of AgNPs shifts the LSPR band, resulting in a visible change in colour [104].

2.B.4.7.2 Sensor performance metrics

The LOD was estimated using RGB values which were obtained from the previous method stated in section 2.B.4.1.2. A calibration graph was plotted with the ratio [G/(R+G+B)] against the concentration of lead ion, as it resulted in a linear relationship. A linearly calibrated plot was necessary for calculation of LOD. This graph facilitated the determination of the LOD using the specified formula, which was found to be 0.35 ppm [93-95] (**Fig. 2.B.21**).

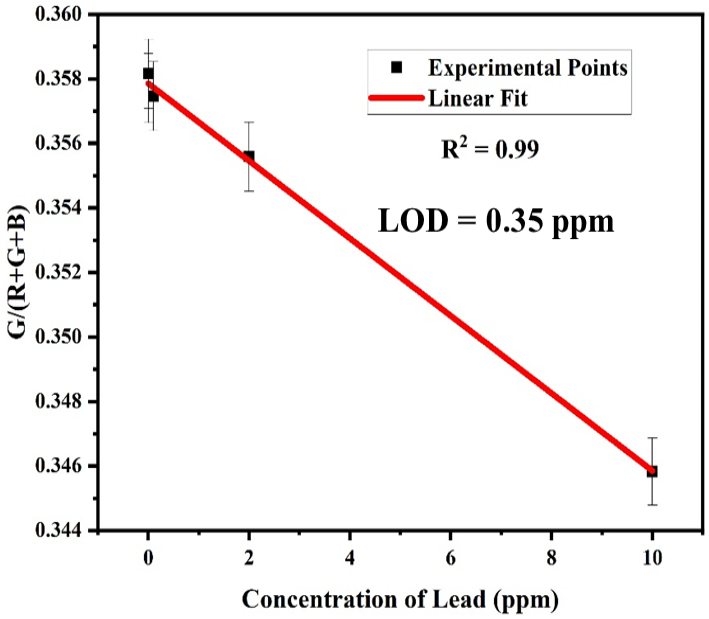

Figure 2.B.21: *Calibration curve for lead adulterated milk.*

2.B.5 Simultaneous sensing of multiple adulterants and contaminants in the paper-based platform

For detection, milk needs to be pretreated to remove the interfering fats and proteins as they may cause hindrance in the detection process. After successful pretreatment, the milk supernatant is used for further detection, by pouring it at the centre of the paper substrate, which flows through all the channels/conduits interacting with the selectively functionalized NPs at the leg ends. When unadulterated and uncontaminated milk was poured, the interaction resulted in no colorimetric change. However, if the milk was adulterated/ contaminated with a specific adulterant/ contaminant, visible colour change was observed at that particular leg end.

Simultaneous detection occurs when 5 mL of milk contaminated with various adulterants and contaminants was introduced, causing colour changes in all channel ends. The response time typically ranges from 5 to 20 min, depending on the concentration of analytes present. A higher concentration leads to a quicker colour change, while lower concentrations extend the response time up to 20 min, considered as the standard response time for sensing. In cases where specific adulterants or contaminants are present, the colour change occurs selectively in the corresponding channel end designed for detecting that particular analyte. The standard response time remains consistent at 20 min for these selective detections. When milk was free from all seven analytes, there was no observable colour change at the end of each channel where the NPs were localized.

When melamine adulterated milk was poured, the colour of the functionalised NPs attached to the corresponding to the leg end changes to purple when higher amount of melamine was present (50 to 100 ppm), to brown (10 to 40 ppm) and to red (0.001 to 8 ppm).

For formalin adulterated milk the colour of NPs changes to dark blackish brown when higher amount of formalin was present (148 to 370000 ppm), and to black (0.37 to 148 ppm).

For hydrogen peroxide adulterated milk, the colour of NPs changes to colourless when higher amount of hydrogen peroxide was present (150 to 300000 ppm), and to pale yellow (0.003 to 120 ppm).

For mercury contaminated milk the colour of NPs changes to colourless when higher amount of mercury was present (60 to 100 ppm), to occur (8 to 50 ppm), and to light brown (0.0001 to 6 ppm).

For arsenic contaminated milk the colour of NPs changes to bluish black when higher amount of arsenic was present (8 to 100 ppm), to red (1 to 6 ppm), and to orange (0.001 to 0.1 ppm).

For cadmium contaminated milk the colour of the functionalised NPs changes to bluish black when higher amount of cadmium was present (30 to 100 ppm), to red (1 to 20 ppm), and to orange (0.001 to 0.1 ppm).

For lead the colour of the functionalised NPs changes to dark agglomerated brown when higher amount of lead was present (100 to 1000 ppm), to purple (70 to 190 ppm) and to red (0.001 to 60 ppm).

The fabricated device offers a qualitative assessment of various adulterants, including melamine, hydrogen peroxide, and formalin, as well as contaminants such as mercury, arsenic, lead, and cadmium in milk. It achieves this by displaying colour changes in the substrate, which contains selectively functionalized NPs for detecting each specific adulterant and contaminant (**Fig. 2.B.22**).

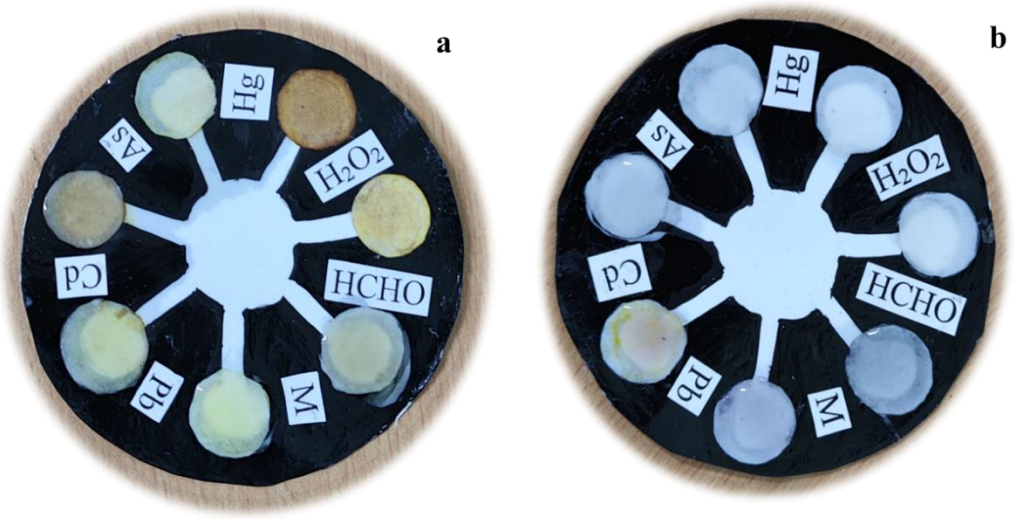

Figure 2.B.22: *Upon addition of* ***(a)*** *unadulterated or uncontaminated milk, and* ***(b)*** *adulterated or contaminated milk.*

2.B.6 Conclusion

The work reports a novel paper-based sensing platform that uses multiple functionalized NPs for the simultaneous sensing of various adulterants and contaminants. This platform features seven conduits, each end selectively impregnated with specific functionalized NPs, separated by hydrophobic barriers. When adulterated or contaminated milk is poured, the resulting colour changes at the conduit ends indicate the presence of specific adulterants. This sensing architecture is specifically designed to detect melamine, formalin, and hydrogen peroxide as adulterants, and mercury, arsenic, cadmium, and lead as contaminants, with each sensing scheme could detect the presence of these adulterants with LOD of 0.76 ppm, 4.53 ppm, 5.6 ppm, 0.87 ppm, 0.65 ppm, 0.73 ppm and 0.35 ppm for melamine, formalin, hydrogen peroxide, mercury ion, arsenic ion, cadmium ion and lead ion respectively, with remarkable sensitivity.

References

[1]https://timesofindia.indiatimes.com/blogs/toi-editorials/adulteration-central [Accessed on 28 September 2024].

[2] Azad, T., and Ahmed, S. Common milk adulteration and their detection techniques. *International Journal of Food Contamination*, 3: 1-9, 2016.

[3] Boudebbouz, A., Boudalia, S., Bousbia, A., Habila, S., Boussadia, M. I., and Gueroui, Y. Heavy metals levels in raw cow milk and health risk assessment across the globe: A systematic review. *Science of the total Environment*, 751: 141830, 2021.

[4] Nascimento, C. F., Santos, P. M., Pereira-Filho, E. R., and Rocha, F. R. Recent advances on determination of milk adulterants. *Food chemistry*, 221: 1232-1244, 2017.

[5] Singh, P., and Gandhi, N. Milk preservatives and adulterants: processing, regulatory and safety issues. *Food Reviews International*, 31(3): 236-261, 2015.

[6] Yadav, A. K., Gattupalli, M., Dashora, K., and Kumar, V. Key milk adulterants in India and their detection techniques: A review. *Food Analytical Methods*, 16(3): 499-514, 2013.

[7] Haji, A., Desalegn, K., and Hassen, H. Selected food items adulteration, their impacts on public health, and detection methods: A review. *Food Science & Nutrition*, 11(12): 7534-7545, 2023.

[8] Alinezhad, Z., Hashemi, M., and Tavakoly Sany, S. B. Concentration of heavy metals in pasteurized and sterilized milk and health risk assessment across the globe: A systematic review. *Plos one*, 19(2): e0296649, 2024.

[9] Beikzadeh, S., Ebrahimi, B., Mohammadi, R., Beikzadeh, M., Asghari-Jafarabadi, M., and Foroumandi, E. Heavy metal contamination of milk and milk products consumed in Tabriz. *Current nutrition & food science*, 15(5): 484-492, 2019.

[10] Ismail, A., Riaz, M., Akhtar, S., Goodwill, J. E., and Sun, J. Heavy metals in milk: global prevalence and health risk assessment. *Toxin Reviews*, 38(1): 1-12, 2019.

[11] Putri, L. A., Prabowo, Y. D., Dewi, D. M. M., Mumtazah, Z., Adila, F. P., Fadillah, G., ... and Wasisto, H. S. Review of Noble Metal Nanoparticle-Based Colorimetric Sensors for Food Safety Monitoring. *ACS Applied Nano Materials*, 7(17): 19821–19853, 2024.

[12] Hang, Y., Wang, A., and Wu, N. Plasmonic silver and gold NPs: shape-and structure-modulated plasmonic functionality for point-of-caring sensing, bio-imaging and medical therapy. *Chemical Society Reviews*, 53: 2932-2971, 2024.

[13] Aminu, A., and Oladepo, S. A. Fast orange peel-mediated synthesis of AgNPs and use as visual colorimetric sensor in the selective detection of mercury (II) ions. *Arabian Journal for Science and Engineering*, 46(6): 5477-5487, 2021.

[14] Nguyen, N. P. U., Dang, N. T., Doan, L., and Nguyen, T. T. H. Synthesis of silver NPs: from conventional to 'modern'methods—a review. *Processes*, 11(9): 2617, 2023.

[15] Poonia, A., Jha, A., Sharma, R., Singh, H. B., Rai, A. K., and Sharma, N. Detection of adulteration in milk: A review. *International journal of dairy technology*, 70(1): 23-42, 2017.

[16] Song, J., Wu, F., Wan, Y., and Ma, L. Colorimetric detection of melamine in pretreated milk using silver NPs functionalized with sulfanilic acid. *Food Control*, 50: 356-361, 2015.

[17] Rajput, J. K. Bio-polyphenols promoted green synthesis of silver NPs for facile and ultra-sensitive colorimetric detection of melamine in milk. *Biosensors and Bioelectronics*, 120: 153-159, 2018.

[18] Farrokhnia, M., Karimi, S., and Askarian, S. Strong hydrogen bonding of gallic acid during synthesis of an efficient AgNPs colorimetric sensor for melamine detection via dis-synthesis strategy. *ACS Sustainable Chemistry & Engineering*, 7(7): 6672-6684, 2019.

[19] Alam, M. F., Laskar, A. A., Ahmed, S., Shaida, M. A., and Younus, H. Colorimetric method for the detection of melamine using in-situ formed silver NPs via tannic acid. *Spectrochimica Acta Part A: Molecular and Biomolecular Spectroscopy*, 183: 17-22, 2017.

[20] Song, J., Wu, F., Wan, Y., and Ma, L. H. Visual test for melamine using silver NPs modified with chromotropic acid. *Microchimica Acta*, 181: 1267-1274, 2014.

[21] Singh, R., Mehra, R., Walia, A., Gupta, S., Chawla, P., Kumar, H., and Kumar, N. Colorimetric sensing approaches based on silver NPs aggregation for determination of toxic metal ions in water sample: a review. *International Journal of Environmental Analytical Chemistry*, 103(6): 1361-1376, 2023.

[22] Tang, L., and Li, J. Plasmon-based colorimetric nanosensors for ultrasensitive molecular diagnostics. *ACS sensors*, 2(7): 857-875, 2017.

[23] Ma, Y., Niu, H., Zhang, X., and Cai, Y. One-step synthesis of silver/dopamine NPs and visual detection of melamine in raw milk. *Analyst*, 136(20): 4192-4196, 2011.

[24] Shellaiah, M., and Sun, K. W. Review on anti-aggregation-enabled colorimetric sensing applications of gold and silver NPs. *Chemosensors*, 10(12): 536, 2024.

[25] Mao, L., Wang, Q., Luo, Y., and Gao, Y. Detection of Ag+ ions via an anti-aggregation mechanism using unmodified gold NPs in the presence of thiamazole. *Talanta*, 222: 121506, 2021.

[26] Han, C., and Li, H. Visual detection of melamine in infant formula at 0.1 ppm level based on silver NPs. *Analyst*, 135(3): 583-588, 2010.

[27] Martínez-Aquino, C., Costero, A. M., Gil, S., and Gaviña, P. Resorcinol functionalized gold NPs for formaldehyde colorimetric detection. *Nanomaterials*, 9(2): 302, 2019.

[28] Teodoro, K. B., Migliorini, F. L., Christinelli, W. A., and Correa, D. S. Detection of hydrogen peroxide (H2O2) using a colorimetric sensor based on cellulose nanowhiskers and silver NPs. *Carbohydrate polymers*, 212: 235-241, 2019.

[29] Aftab, R., Ahsan, S., Liaqat, A., Safdar, M., Chughtai, M. F. J., Nadeem, M., ... and Khaliq, A. Green-synthesized selenium NPs using garlic extract and their application for rapid detection of salicylic acid in milk. *Food Science and Technology*, 43: e67022, 2023.

[30] Gao, N., Huang, P., and Wu, F. Colorimetric detection of melamine in milk based on Triton X-100 modified gold NPs and its paper-based application. *Spectrochimica Acta Part A: Molecular and Biomolecular Spectroscopy*, 192: 174-180, 2018.

[31] Mirzaei, Y., Gholami, A., Sheini, A., and Bordbar, M. M. An origami-based colorimetric sensor for detection of hydrogen peroxide and glucose using sericin capped silver NPs. *Scientific Reports*, 13(1): 7064, 2023.

[32] Seebunrueng, K., Naksen, P., Jarujamrus, P., Sansuk, S., Treekamol, Y., Teshima, N., Murakami, H., and Srijaranai, S. A sensitive paper-based vapor-test kit for instant formalin detection in food products. *Food Chemistry*, 451: 139402, 2024.

[33] Shrivas, K., Kant, T., Patel, S., Devi, R., Dahariya, N. S., Pervez, S., Deb, M. K., Rai, M. K., and Rai, J. Inkjet-printed paper-based colorimetric sensor coupled with smartphone for determination of mercury (Hg^{2+}). *Journal of Hazardous materials*, 414: 125440, 2021.

[34] Wi, E., and Kim, Y. Highly selective paper-based and colorimetric detection for arsenic (V) with methylene blue-functionalized AuNPs. *Journal of Industrial and Engineering Chemistry*, 124:481-489, 2023.

[35] Wang, H., Da, L., Yang, L., Chu, S., Yang, F., Yu, S., and Jiang, C. Colorimetric fluorescent paper strip with smartphone platform for quantitative detection of cadmium ions in real samples. *Journal of hazardous materials*, 392: 122506, 2020.

[36] Sahu, B., Kurrey, R., Deb, M. K., Shrivas, K., Karbhal, I., and Khalkho, B. R. A simple and cost-effective paper-based and colorimetric dual-mode detection of arsenic (iii) and

lead (ii) based on glucose-functionalized gold NPs. *RSC advances*, 11(34): 20769-20780, 2021.

[37] Guinati, B. G., Sousa, L. R., Oliveira, K. A., and Coltro, W. K. Simultaneous analysis of multiple adulterants in milk using microfluidic paper-based analytical devices. *Analytical Methods*, 13(44): 5383-5390, 2021.

[38] Patari, S., Datta, P., and Mahapatra, P. S. 3d paper-based milk adulteration detection device. *Scientific Reports*, 12(1):13657, 2022.

[39] Singh, P., Singh, S., & Nara, S. Nanotechnology as a tool for contaminants detection in milk or milk products. *Nanomaterials and Nanotechnology: Biomedical, Environmental, and Industrial Applications*, 2021: 133-161, 2021.

[40] Kharabi Masooleh, A., Ahmadikhah, A., and Saidi, A. Green synthesis of stable silver NPs by the main reduction component of green tea (Camellia sinensis L.). *IET anobiotechnology*, 13(2): 183-188, 2019.

[41] Xing, H. B., Wu, Y. G., Zhan, S. S., and Zhou, P. A rapid colorimetric detection of melamine in raw milk by unmodified gold NPs. *Food Analytical Methods*, 6: 1441-1447, 2013.

[42] Gloria, E. C., Ederley, V., Gladis, M., César, H., Jaime, O., Oscar, A., ... and Franklin, J. Synthesis of silver NPs (AgNPs) with antibacterial activity. *In Journal of Physics: Conference Series*, 850(1): 012023, 2017.

[43] Babu, S. A., & Prabu, H. G. Synthesis of AgNPs using the extract of Calotropis procera flower at room temperature. Materials Letters, 65(11): 1675-1677, 2011.

[44] Wu, M., Guo, H., Liu, L., Liu, Y., and Xie, L. Size-dependent cellular uptake and localization profiles of silver NPs. *International journal of nanomedicine*, 2019: 4247-4259, 2019.

[45] Premkumar, J., Sudhakar, T., Dhakal, A., Shrestha, J. B., Krishnakumar, S., and Balashanmugam, P. Synthesis of silver NPs (AgNPs) from cinnamon against bacterial pathogens. *Biocatalysis and agricultural biotechnology*, 15: 311-316, 2018.

[46] Widatalla, H. A., Yassin, L. F., Alrasheid, A. A., Ahmed, S. A. R., Widdatallah, M. O., Eltilib, S. H., and Mohamed, A. A. (2022). Green synthesis of silver NPs using green tea leaf extract, characterization and evaluation of antimicrobial activity. *Nanoscale Advances*, 4(3): 911-915, 2022.

[47] Nandiyanto, A. B. D., Oktiani, R., and Ragadhita, R. How to read and interpret FTIR spectroscope of organic material. *Indonesian Journal of Science and Technology*, 4(1): 97-118, 2019.

[48] Zhao, Y., Tian, Y., Ma, P., Yu, A., Zhang, H., and Chen, Y. Determination of melamine and malachite green by surface-enhanced Raman scattering spectroscopy using starch-coated silver NPs as substrates. *Analytical Methods*, 7(19): 8116-8122, 2015.

[49] Gopal, J., Muthu, M., Paul, D., Kim, D. H., and Chun, S. Bactericidal activity of green tea extracts: the importance of catechin containing nano particles. *Scientific Reports*, 6(1): 19710, 2016.

[50] Singh, B. N., Shankar, S., and Srivastava, R. K. Green tea catechin, epigallocatechin-3-gallate (EGCG): mechanisms, perspectives and clinical applications. *Biochemical pharmacology*, 82(12): 1807-1821, 2011.

[51] Varun, S., Daniel, S. K., and Gorthi, S. S. Rapid sensing of melamine in milk by interference green synthesis of silver NPs. *Materials Science and Engineering C*, 74: 253-258, 2017.

[52] Li, N., Liu, T., Liu, S. G., Lin, S. M., Fan, Y. Z., Luo, H. Q., and Li, N. B. Visible and fluorescent detection of melamine in raw milk with one-step synthesized silver nanoparticles using carbon dots as the reductant and stabilizer. *Sensors and Actuators B: Chemical*, 248, 597-604, 2017.

[53] Bezuneh, T. T., Ofgea, N. M., Tessema, S. S., and Bushira, F. A. Tannic Acid-Functionalized Silver NPs as Colorimetric Probe for the Simultaneous and Sensitive Detection of Aluminum (III) and Fluoride Ions. *ACS omega*, 8(40): 37293-37301, 2023.

[54] Daniel, S. K., Julius, L. A. N., and Gorthi, S. S. Instantaneous detection of melamine by interference biosynthesis of silver NPs. *Sensors and Actuators B: Chemical*, 238: 641-650, 2017.

[55] Wu, Z., Chen, X., Zhu, S., Zhou, Z., Yao, Y., Quan, W., and Liu, B. Enhanced sensitivity of ammonia sensor using graphene/polyaniline nanocomposite. *Sensors and Actuators B: Chemical*, 178: 485-493, 2013.

[56] Ai, K., Liu, Y., and Lu, L. Hydrogen-bonding recognition-induced color change of gold NPs for visual detection of melamine in raw milk and infant formula. *Journal of the American Chemical Society*, 131(27): 9496-9497, 2009.

[57] Ping, H., Zhang, M., Li, H., Li, S., Chen, Q., Sun, C., and Zhang, T. Visual detection of melamine in raw milk by label-free silver NPs. *Food control*, 23(1): 191-197, 2012.

[58] Giovannozzi, A M., Rolle, F., Sega, M., Abete, M. C., Marchis, and D. Rossi, A. M. Rapid and sensitive detection of melamine in milk with gold NPs by Surface Enhanced Raman Scattering. *Food chemistry*, 159: 250-256, 2014.

[59] Chang, K., Wang, S., Zhang, H., Guo, Q., Hu, X., Lin, Z., Sun, H., Jiang, M., and Hu, J. Colorimetric detection of melamine in milk by using gold NPs-based LSPR via optical fibers, *PLoS One*, 12(5): e0177131, 2017.

[60] Oh, S. Y., Lee, M. J., Heo, N. S., Kim, S., Oh, J. S., Lee, Y., Jeon, E. J., Moon, H., Kim, H. S., Park, T. J., Moon, G., Chun, H. S., and Huh, Y. S. Cuvette-type LSPR sensor for highly sensitive detection of melamine in infant formulas. *Sensors*, 19(18): 383, 2019.

[61] Saha, B. K., Ali, M. Y., Chakraborty, M., Islam, Z., and Hira, A. K. Study on the preservation of raw milk with hydrogen peroxide (HO). *Pakistan Journal of Nutrition*, 2(1): 36-42, 2003.

[62] Dhaka, A., Mali, S. C., Sharma, S., and Trivedi, R. A review on biological synthesis of silver nanoparticles and their potential applications. *Results in Chemistry*, 6: 101108, 2023.

[63] Fernández-Castro, P., Vallejo, M., San Román, M. F., and Ortiz, I. Insight on the fundamentals of advanced oxidation processes. Role and review of the determination methods of reactive oxygen species. *Journal of Chemical Technology & Biotechnolog***y**, 90(5): 796-820, 2015.

[64] Abbas, M. E., Luo, W., Zhu, L., Zou, J., and Tang, H. Fluorometric determination of hydrogen peroxide in milk by using a Fenton reaction system. *Food chemistry*, 120(1): 327-331, 2010.

[65] Raunmoon, S., Sachak, S., Thong-in, W., Sonkhayan, B., Nasomjai, P., Khamai, P., Thim-uam, A., Khwanchaic, P., Tooa, C. O., and Chartarrayawadee, W. Cotton tree (Bombax ceiba L.) flower stamen extract: Turning a food ingredient into a reducing agent for the green synthesis of silver NPs. *ScienceAsia*, 50(1), 2024.

[66] Safdar, M., Aslam, S., Akram, M., Khaliq, A., Ahsan, S., Liaqat, A., Mirza, M., Waqas, M., and Qureshi, W. A. Bombax ceiba flower extract mediated synthesis of Se nanoparticles for antibacterial activity and urea detection. *World Journal of Microbiology and Biotechnology*, 39(3): 80, 2023.

[67] Meeran, M. B. A., Bijili, A. F., and Khader, R. A. A. Evaluation of Corrosion Mitigation Behaviour of Bombax ceiba Leaves Extract. *Applied Biochemistry and Biotechnology*, 195(6): 3787-3806, 2023.

[68] Amirjani, A., Bagheri, M., Heydari, M., and Hesaraki, S. Label-free surface plasmon resonance detection of hydrogen peroxide; a bio-inspired approach. *Sensors and Actuators B: Chemical*, 227: 373-382, 2016.

[69] Zhang, L., and Li, L. Colorimetric detection of hydrogen peroxide using silver NPs with three different morphologies. *Analytical Methods*, 8(37): 6691-6695, 2016.

[70] Nitinaivinij, K., Parnklang, T., Thammacharoen, C., Ekgasit, S., and Wongravee, K. Colorimetric determination of hydrogen peroxide by morphological decomposition of silver nanoprisms coupled with chromaticity analysis. *Analytical Methods*, 6(24), 9816-9824, 2014.

[71] Verma, T., Aggarwal, A., Tripathi, A. D., Rai, D. C., and Jaspal, S. Preservation approaches for milk and milk products: A Review. *Indian Journal of Dairy Science*, 75(5): 2022.

[72] Li, Y., Ou, J., Huang, C., Liu, F., Ou, S., and Zheng, J. Chemistry of formation and elimination of formaldehyde in foods. *Trends in Food Science & Technology*, 104134, 2023.

[73] Adnan, S., Kalwar, N. H., Abbas, M. W., Soomro, R. A., Saand, M. A., Awan, F. R., Avci, A., Pehlivan, E., and Bajwa, S. Enzyme-free colorimetric sensing of glucose using l-cysteine functionalized AgNPs. SN Applied Sciences, 1: 1-9, 2019.

[74] Ankireddy, S. R., and Kim, J. Selective detection of dopamine in the presence of ascorbic acid via fluorescence quenching of InP/ZnS quantum dots. *International journal of nanomedicine*, 10(1): 113-119, 2015.

[75] Kallen, R. G. Mechanism of reactions involving Schiff base intermediates. Thiazolidine formation from L-cysteine and formaldehyde. *Journal of the American Chemical Society*, 93(23): 6236-6248, 1971.

[76] Kallen, R. G. Equilibriums for the reaction of cysteine and derivatives with formaldehyde and protons. *Journal of the American Chemical Society*, 93(23): 6227-6235, 1971.

[77] Boruah, B. S., Daimari, N. K., and Biswas, R. Functionalized silver nanoparticles as an effective medium towards trace determination of arsenic (III) in aqueous solution. *Results in Physics*, 12: 2061-2065, 2019.

[78] Ionescu, A. D., Cîrîc, A. I., and Begea, M. A review of milk frauds and adulterations from a technological perspective. *Applied Sciences*, 13(17): 9821, 2023.

[79] Alberti, G., Zanoni, C., Magnaghi, L. R., and Biesuz, R. Gold and silver nanoparticle-based colorimetric sensors: New trends and applications. *Chemosensors*, 9(11): 305, 2021.

[80] Ndikau, M., Noah, N. M., Andala, D. M., and Masika, E. Green synthesis and characterization of silver NPs using Citrullus lanatus fruit rind extract. *International Journal of Analytical Chemistry*, 2017(1): 8108504, 2017.

[81] Lakshmipathy, R., and Sarada, N. C. Methylene blue adsorption onto native watermelon rind: batch and fixed bed column studies. *Desalination and Water Treatment*, 57(23): 10632-10645, 2016.

[82] Mamiru, D., and Gonfa, G. Extraction and characterization of pectin from watermelon rind using acetic acid. *Heliyon*, 9(2), 2023.

[83] Zulkifli, N. I., Muhamad, M., Mohamad Zain, N. N., Tan, W. N., Yahaya, N., Bustami, Y., Abdul, A. A., and Nik Mohamed Kamal, N. N. S. A bottom-up synthesis approach to silver NP induces anti-proliferative and apoptotic activities against MCF-7, MCF-7/TAMR-1 and MCF-10A human breast cell lines. *Molecules*, 25(18); 4332, 2020.

[84] AMohan, A., and Shanmugam, S. Comparison of the nutritional, physico-chemical and anti-nutrient properties of freeze and hot air-dried watermelon (Citrullus Lanatus) rind. *Biosciences Biotechnology Research Asia*, 13(2): 1113-1119, 2016.

[85] Vilela, D., González, M. C., and Escarpa, A. Sensing colorimetric approaches based on gold and silver NPs aggregation: Chemical creativity behind the assay. A review. *Analytica chimica acta*, 751: 24-43, 2012.

[86] Samoilova, N., Krayukhina, M., Naumkin, A., Anuchina, N., and Popov, D. Silver NPs doped with silver cations and stabilized with maleic acid copolymers: Specific structure and antimicrobial properties. *New Journal of Chemistry*, 45(32): 14513-14521, 2021.

[87] Wirwis, A., and Sadowski, Z. Green synthesis of silver NPs: optimizing green tea leaf extraction for enhanced physicochemical properties. *ACS omega*, 8(33): 30532-30549, 2023.

[88] Shrivas, K., Sahu, B., Deb, M. K., Thakur, S. S., Sahu, S., Kurrey, R., ... and Jangde, R. Colorimetric and paper-based detection of lead using PVA capped silver NPs: Experimental and theoretical approach. *Microchemical Journal*, 150: 104156, 2019.

[89] Neog, A., Das, P., and Biswas, R. A novel green approach towards synthesis of silver NPs and it's comparative analysis with conventional methods. *Applied Physics A*, 127(12): 913, 2021.

[90] Kalam, A., Al-Sehemi, A. G., Alrumman, S., Du, G., Assiri, M., and Hesham, A. E. L. Antibacterial studies of bio-functionalized carbon decorated silver NPs (AgNPs). *Journal of the Indian Chemical Society*, 98(10): 100155, 2021.

[91] Bano, A. Interactive effects of Ag-nanoparticles, salicylic acid, and plant growth promoting rhizobacteria on the physiology of wheat infected with yellow rust. *Journal of Plant Pathology*, 102(4): 1215-1225, 2020.

[92] Taati, H., Sangani, H., Davoudi, A., Safabakhsh Kouchesfahani, S., Hedayati, M., Tarashandeh Hemmati, S., Ghasemipour, T., Aghajani, S., Farah Andooz, M., Amanollahi, M., Kalavari, F., and Salehzadeh, A. Silver nanoparticle functionalized by glutamine and conjugated with thiosemicarbazide induces apoptosis in colon cancer cell line. *Scientific Reports*, 14(1): 3809, 2024.

[93] Firdaus, M. L., Aprian, A., Meileza, N., Hitsmi, M., Elvia, R., Rahmidar, L., and Khaydarov, R. Smartphone coupled with a paper-based colorimetric device for sensitive and portable mercury ion sensing. *Chemosensors*, 7(2): 25, 2019.

[94] Soda, Y., and Bakker, E. Quantification of colorimetric data for paper-based analytical devices. *ACS sensors*, 4(12): 3093-3101, 2019.

[95] Hamedpour, V., Oliveri, P., Malegori, C., and Minami, T. Development of a morphological color image processing algorithm for paper-based analytical devices. *Sensors and Actuators B: Chemical*, 322: 128571, 2020.

[96] Nguyen, N. D., Van Nguyen, T., Chu, A. D., Tran, H. V., Tran, L. T., and Huynh, C. D. A label-free colorimetric sensor based on silver NPs directed to hydrogen peroxide and glucose. Arabian Journal of Chemistry, 11(7), 1134-1143, 2018.

[97] Jeevika, A., and Shankaran, D. R. Functionalized silver NPs probe for visual colorimetric sensing of mercury. *Materials Research Bulletin*, 83: 48-55, 2016.

[98] Tarim, E. A., and Tekin, H. C. Colorimetric detection of serum creatinine on a miniaturized platform using hue-saturation-value space analysis. *Scientific Reports*, 14(1): 19441, 2024.

[99] Balbach, S., Jiang, N., Moreddu, R., Dong, X., Kurz, W., Wang, C., Dong, J., Yin, Y., Butt, H., Brischwein, M., Hayden, O., Jakobi, M., Tasoglu, S., Koch, A. W. and Yetisen, A. K. Smartphone-based colorimetric detection system for portable health tracking. *Analytical Methods*, 13(38): 4361-4369, 2021.

[100] Kılıç, V., Horzum, N., and Solmaz, M. E. From sophisticated analysis to colorimetric determination: Smartphone spectrometers and colorimetry. *Color Detection*, 1-19, 2018.

[101] Hong, J. I., and Chang, B. Y. Development of the smartphone-based colorimetry for multi-analyte sensing arrays. *Lab on a Chip*, 14(10): 1725-1732, 2014.

[102] Sudarman, F., Shiddiq, M., Armynah, B., and Tahir, D. Silver NPs (AgNPs) synthesis methods as heavy-metal sensors: A review. *International Journal of Environmental Science and Technology*, 20(8); 9351-9368, 2023.

[103] Guo, B., Liu, C., Liang, Y., Li, N., and Fu, Q. Salicylic acid signals plant defence against cadmium toxicity. *International Journal of Molecular Sciences*, 20(12): 2960, 2019.

[104] Kim, H. N., Ren, W. X., Kim, J. S., and Yoon, J. Fluorescent and colorimetric sensors for detection of lead, cadmium, and mercury ions. *Chemical Society Reviews*, 41(8): 3210-3244, 2012.